



**HAL**  
open science

# GJK++: Leveraging Acceleration Methods for Faster Collision Detection

Louis Montaut, Quentin Le Lidec, Vladimír Petřík, Josef Sivic, Justin Carpentier

► **To cite this version:**

Louis Montaut, Quentin Le Lidec, Vladimír Petřík, Josef Sivic, Justin Carpentier. GJK++: Leveraging Acceleration Methods for Faster Collision Detection. IEEE Transactions on Robotics, In press. hal-04070039v2

**HAL Id: hal-04070039**

**<https://hal.science/hal-04070039v2>**

Submitted on 29 Nov 2023 (v2), last revised 3 Apr 2024 (v3)

**HAL** is a multi-disciplinary open access archive for the deposit and dissemination of scientific research documents, whether they are published or not. The documents may come from teaching and research institutions in France or abroad, or from public or private research centers.

L'archive ouverte pluridisciplinaire **HAL**, est destinée au dépôt et à la diffusion de documents scientifiques de niveau recherche, publiés ou non, émanant des établissements d'enseignement et de recherche français ou étrangers, des laboratoires publics ou privés.

# GJK++: Leveraging Acceleration Methods for Faster Collision Detection

Louis Montaut, Quentin Le Lidec, Vladimir Petrik, Josef Sivic and Justin Carpentier

1 **Abstract**—Collision detection is a fundamental problem in  
 2 various domains, such as robotics, computational physics, and  
 3 computer graphics. In general, collision detection is tackled as  
 4 a computational geometry problem, with the so-called Gilbert,  
 5 Johnson, and Keerthi (GJK) algorithm being the most adopted  
 6 solution nowadays. While introduced in 1988, GJK remains the  
 7 most effective solution to compute the distance or the collision  
 8 between two 3D convex geometries. Over the years, it was  
 9 shown to be efficient, scalable, and generic, operating on a  
 10 broad class of convex shapes, ranging from simple primitives  
 11 (sphere, ellipsoid, box, cone, capsule, etc.) to complex meshes  
 12 involving thousands of vertices. In this article, we introduce  
 13 several contributions to accelerate collision detection and distance  
 14 computation between convex geometries by leveraging the fact  
 15 that these two problems are fundamentally optimization problems.  
 16 Notably, we establish that the GJK algorithm is a specific  
 17 sub-case of the well-established Frank-Wolfe (FW) algorithm in  
 18 convex optimization. By adapting recent works linking Polyak  
 19 and Nesterov accelerations to Frank-Wolfe methods, we also  
 20 propose two accelerated extensions of the classic GJK algorithm.  
 21 Through an extensive benchmark over millions of collision pairs  
 22 involving objects of daily life, we show that these two accelerated  
 23 GJK extensions significantly reduce the overall computational  
 24 burden of collision detection, leading to computation times that  
 25 are up to two times faster. Finally, we hope this work will  
 26 significantly reduce the computational cost of modern robotic  
 27 simulators, allowing the speed-up of modern robotic applications  
 28 that heavily rely on simulation, such as reinforcement learning  
 29 or trajectory optimization.

30 **Index Terms**—Convex Optimization, Collision Detection, Com-  
 31 putational Geometry, Computer Graphics, Simulation, Trajec-  
 32 tory Optimization, Motion Planning

## I. INTRODUCTION

34 **P**HYSICS engines designed to simulate rigid bodies are an  
 35 essential tool used in a wide variety of applications, nota-  
 36 bly in robotics, video games, and computer graphics [1]–[3].  
 37 Collision detection, a crucial feature of any physics engine or  
 38 robot motion planner [4]–[6], consists of finding which objects  
 39 are colliding or not, *i.e.* are sharing at least one common point  
 40 or if there exists a separating hyper-plane between both. As  
 41 simulation often needs to deal with multiple objects and run in  
 42 real-time (*i.e.*, in video games) or at very high frequencies (*i.e.*,

Louis Montaut is with Inria, Département d’Informatique de l’École Nor-  
 male Supérieure, PSL Research University in Paris, France and also with the  
 Czech Institute of Informatics, Robotics and Cybernetics in Prague, Czech  
 Republic.

Vladimir Petrik and Josef Sivic are with the Czech Institute of Informatics,  
 Robotics and Cybernetics, Czech Technical University in Prague.

Quentin Le Lidec and Justin Carpentier are with Inria and Département  
 d’Informatique de l’École Normale Supérieure, PSL Research University in  
 Paris, France.

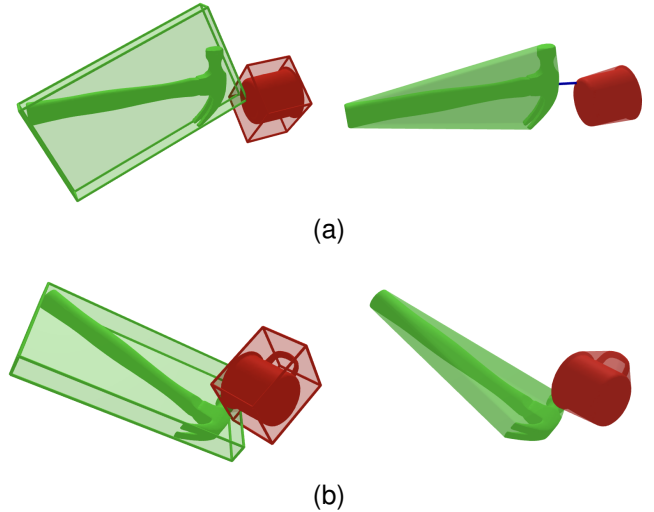


Fig. 1. Two distinct collision problems using shapes from the YCB dataset: in (a) the shapes  $\mathcal{A}_1$  (in green) and  $\mathcal{A}_2$  (in red) are not in collision ( $\text{dist}(\mathcal{A}_1, \mathcal{A}_2) > 0$ ) whereas in (b) the shapes are in collision ( $\text{dist}(\mathcal{A}_1, \mathcal{A}_2) = 0$ ). In the left column, the oriented bounding boxes (OBB) of the objects are represented in light colors. In the right column, the light colors represent the convex hull of each object. In both collision problems, (a) and (b), the broad phase finds a collision between the object’s OBBs; the narrow phase must thus be called to confirm or infirm the collision. The right column corresponds to the narrow phase in which the GJK algorithm is called on the objects’ convex hulls. In this paper, we propose the Polyak-accelerated GJK and Nesterov-accelerated GJK algorithms in order to accelerate collision detection.

in robotics), collision detection must be carried out as fast as  
 possible. To reduce computational times, collision detection is  
 usually decomposed into two phases thoroughly covered in [7].  
 The first phase is the so-called *broad phase* which consists  
 in identifying which pair of simulated objects are potentially  
 colliding. The broad phase relies on the simulated objects’  
 bounding volumes, as shown in Fig. 1, allowing to quickly  
 assess if the objects are *not* in collision. The second phase is  
 the so-called *narrow phase* in which each pair identified in  
 the broad phase is tested to check whether a collision is truly  
 occurring. Collision detection during the narrow phase is the  
 focus of this paper.

**Problem formulation.** We consider two convex shapes  $\mathcal{A}_1$   
 and  $\mathcal{A}_2$  in  $\mathbb{R}^n$  (with  $n = 2$  or  $3$  in common applications).  
 If the shapes are not convex, we use their respective convex  
 hulls or decompose them into a collection of convex sub-  
 shapes [8]. The *separation distance* between  $\mathcal{A}_1$  and  $\mathcal{A}_2$ ,  
 denoted by  $\text{dist}(\mathcal{A}_1, \mathcal{A}_2) \in \mathbb{R}_+$ , can be formulated as a

1 minimization problem of the form:

$$d_{1,2} = \min_{\mathbf{x}_1 \in \mathcal{A}_1, \mathbf{x}_2 \in \mathcal{A}_2} \|\mathbf{x}_1 - \mathbf{x}_2\|^2 \quad (1)$$

and  $\text{dist}(\mathcal{A}_1, \mathcal{A}_2) = \sqrt{d_{1,2}}$ ,

2 where  $\mathbf{x}_1 \in \mathcal{A}_1$  and  $\mathbf{x}_2 \in \mathcal{A}_2$  are both vectors in  $\mathbb{R}^n$ ,  $d_{1,2}$   
 3 is the optimal value of (1) and  $\|\cdot\|$  is the Euclidian norm  
 4 of  $\mathbb{R}^n$ . If  $\mathcal{A}_1$  and  $\mathcal{A}_2$  intersect (*i.e.*, they are in collision),  
 5 we necessarily have  $\text{dist}(\mathcal{A}_1, \mathcal{A}_2) = 0$ . If the two shapes do  
 6 not intersect, we have  $\text{dist}(\mathcal{A}_1, \mathcal{A}_2) > 0$ . These two cases are  
 7 illustrated in Fig. 1.

8 Problem (1) allows us to consider both the *distance com-*  
 9 *putation* problem and the computationally cheaper *Boolean*  
 10 *collision check* as one single convex optimization problem. In  
 11 the distance computation problem, we aim at computing the  
 12 separation distance between  $\mathcal{A}_1$  and  $\mathcal{A}_2$ , denoted  $\text{dist}(\mathcal{A}_1, \mathcal{A}_2)$ ,  
 13 *i.e.* the distance between their closest points. This distance  
 14 is helpful in some applications such as collision-free path  
 15 planning [9], [10], especially for pairs of objects entering the  
 16 narrow phase. If the broad phase has not selected a pair of  
 17 objects, a cheap estimate of  $\text{dist}(\mathcal{A}_1, \mathcal{A}_2)$  is usually enough [7].  
 18 In the Boolean collision check, we only aim at determin-  
 19 ing if  $\mathcal{A}_1$  and  $\mathcal{A}_2$  intersect, and computing  $\text{dist}(\mathcal{A}_1, \mathcal{A}_2)$  is  
 20 unnecessary. However, we will later see that the Boolean  
 21 collision check is a sub-problem of the distance computation  
 22 problem: solving (1) can be early-stopped once a separating  
 23 plane between  $\mathcal{A}_1$  and  $\mathcal{A}_2$  has been found. In the rest of this  
 24 paper, we will use the generic term “collision detection” to  
 25 refer to distance computation and Boolean collision checking  
 26 altogether. We will specify when the distinction is needed.

27 **Contributions and paper outline.** Our work builds on the  
 28 seminal works by [11] and [12] as well as on the work of [13],  
 29 [14] to globally accelerate distance computation and collision  
 30 checking algorithms between convex shapes. We make the  
 31 following contributions:

- 32  $\hookrightarrow$  In Sec. II, we provide an in-depth tutorial on the state-of-  
 33 the-art Gilbert-Johnson-Keerthi (GJK) algorithm used to  
 34 solve collision detection problems. Although it is often  
 35 presented and discussed as a computational geometry  
 36 algorithm, we show that GJK is, in fact, a sub-case of the  
 37 much older fully-corrective Frank-Wolfe (FW) algorithm;
- 38  $\hookrightarrow$  In Sec. III, we adapt recent works on Polyak and  
 39 Nesterov-accelerated FW to accelerate both the distance  
 40 computation and the Boolean collision check problems;
- 41  $\hookrightarrow$  In Sec. IV, we empirically analyze the convergence of  
 42 our proposed approach on two large shape benchmarks.  
 43 Results show a faster convergence of our approach lead-  
 44 ing to a computational time up to two times faster than  
 45 the state-of-the-art GJK algorithm on both distance com-  
 46 putation and Boolean collision checking. We also provide  
 47 a benchmark against other collision detection algorithms  
 48 from the libCCD [15], FCL [16] and BulletCollision [17]  
 49 collision detection libraries which are used in physics  
 50 simulators like Drake [18], MuJoCo [3], ODE [19] and  
 51 Bullet [1].
- 52  $\hookrightarrow$  We empirically show that GJK-like algorithms, which our  
 53 proposed methods belong to, are superior by orders of

magnitude to generic quadratic programming solvers on  
 collision detection problems;

- $\hookrightarrow$  Finally, we show that our methods can be used in any  
 physics simulator by benchmarking them on trajectories  
 generated by the Bullet simulator. Like GJK, our methods  
 can benefit from being warm-started using the previous  
 simulation time steps, enabling temporal coherence for  
 our proposed accelerated collision detection algorithms.

This article is an extended version of a previously published  
 paper [20] which presented the Nesterov-accelerated GJK  
 algorithm. To expand on our previous work, we introduce the  
 Polyak-accelerated GJK algorithm, provide additional bench-  
 marks, notably against existing collision detection libraries,  
 and show that our proposed methods can be used in the context  
 of physics simulation by benefiting from being warm-started  
 using previous simulation steps.

In the rest of this section, we first formulate the problem of  
 collision detection and then provide an overview of collision  
 detection related works.

**Related work.** The so-called Gilbert-Johnson-Keerthi algo-  
 rithm (GJK) [12] is the most well-known algorithm for colli-  
 sion detection between two convex shapes. It can handle the  
 distance computation and the Boolean collision check [21].  
 The expanding polytope algorithm (EPA) [22], an extension  
 to GJK, can compute the penetration depth *i.e.* the norm of the  
 separation vector, when shapes are in collision. The separation  
 vector is the vector of smallest norm needed to translate one of  
 the two shapes such that the two shapes do not intersect. The  
 EPA solves a non-convex and more complex problem than (1),  
 which is not the focus of this paper.

Most alternatives to GJK in the literature focus on com-  
 puting collisions between convex polyhedra, such as the Lin-  
 Canny algorithm [23] or the V-Clip [24] algorithm. Although  
 GJK is equivalent in performance to these algorithms [25],  
 it is not restricted to convex polyhedra. The strength of  
 GJK is formulating the collision detection problem on the  
 Minkowski difference. The properties of the Minkowski dif-  
 ference are used to cleverly compute support vectors on  
 the Minkowski difference (these notions are introduced and  
 detailed in Sec. II). GJK can thus handle collision detection,  
 and distance computation for many different shapes such as  
 convex polyhedra and basic primitives (*i.e.*, spheres, ellipsoids,  
 cylinders, capsules etc.) [7], [21], [26]. The Minkowski Portal  
 Refinement (MPR) [27] is a variant of the GJK algorithm  
 which is slightly simpler to implement; however, MPR can  
 only perform boolean collision checks as it cannot be used  
 to perform distance computation between non-overlapping  
 shapes. Overall, the generality of GJK, efficiency, good preci-  
 sion, and ease of implementation make it the state-of-the-art  
 algorithm for collision detection between two convex shapes.

Collision detection has been casted into a convex opti-  
 mization problem for many years [12], [28], [29]. However,  
 collision detection is traditionally presented and considered  
 mainly as a computational geometry problem [7], [21], [24],  
 [25], [30], [31]. Over the years, this computational geometric  
 perspective allowed enhancing the computational efficiency of  
 GJK, thanks to improvements to its internal sub-routines [21],

[30]. However, we argue that this view has also limited collision detection improvement. Instead, we propose to tackle collision from the perspective of convex optimization. This correlates with some observations raised in the original GJK papers. Indeed, as briefly mentioned already in their 1988 paper [12] and brought up again by [29], [32], the ideas developed by Gilbert, Johnson, and Keerthi are rooted in convex optimization, notably in the works of [33] and [34] for solving Minimum-Norm Point (MNP) problems. This article proposes exploiting the Frank-Wolfe convex optimization setting to tackle collision detection. In particular, by leveraging recent progresses in acceleration methods in convex optimization [35], we show how to accelerate collision detection by directly lowering the number of iterations needed to solve a collision problem instance compared to the vanilla GJK algorithm.

The Frank-Wolfe algorithm (FW) dates back to 1956 and is one of the first convex optimization algorithms. It has been heavily studied over the years by the optimization community. This algorithm iterates over the computation of *support points* to approach the optimal solution. The undesired zig-zagging behavior of FW, already identified by its authors, has been addressed by introducing corrections to the original FW method [33], [34], [36]–[40]. In [38] and [40], widely used corrections of the FW algorithm are analyzed, and their convergence properties. In this work, we notably show in Sec. II that the GJK algorithm is an instance of the *fully-corrective* Frank-Wolfe algorithm, covered in [40], applied to solving a MNP problem. Finally, recent works have also tried accelerating the FW algorithm by applying the so-called Nesterov acceleration [41], a classic acceleration technique in unconstrained optimization. Nesterov momentum has been successfully added by [14] to accelerate FW.

## II. COLLISION DETECTION FROM A FRANK-WOLFE PERSPECTIVE

In this section, we highlight the natural connection between computing the distance between convex shapes and convex optimization, particularly within the frame of the Frank-Wolfe (FW) setting. The first part of this section is a tutorial on collision detection, starting with FW and gradually working towards GJK. We then show that the GJK algorithm can be seen as a variant of the FW algorithm that leverages properties of convex 3D shapes to lower the computational complexity drastically.

**Distance computation and Boolean collision checking.** As recalled in Sec. I, collision detection is a sub-case of distance computation:  $\text{dist}(\mathcal{A}_1, \mathcal{A}_2) > 0$  means that the two shapes do not overlap while  $\text{dist}(\mathcal{A}_1, \mathcal{A}_2) = 0$  means that the shapes are in collision. In the case of  $\text{dist}(\mathcal{A}_1, \mathcal{A}_2) > 0$ , finding a strictly positive lower bound on  $d_{1,2}$  to solve the collision problem is sufficient. In the context of convex shapes, this is often simpler than computing the distance between the two shapes [10] and can be done by finding a plane separating  $\mathcal{A}_1$  from  $\mathcal{A}_2$ . In the rest of the paper, we focus on

the generic problem of computing the distance between  $\mathcal{A}_1$  and  $\mathcal{A}_2$ , as it encapsulates the more straightforward Boolean collision check covered later in this section. Results for the particular Boolean collision checking case are analyzed in the experimental section IV.

**Collision detection from the perspective of quadratic programming.** From the perspective of numerical optimization, the first idea is to look at problem (1) through the lens of quadratic programming. In the case of meshes, which are shapes represented by soups of 3D points and which faces represented as triangles, we can use the implicit description of a convex mesh as a linear inequality of the form  $Ax \leq b$ . The collision detection problem between two meshes can thus be cast as a quadratic programming (QP) problem:

$$\begin{aligned} d_{1,2} = \min_{\mathbf{x}_1, \mathbf{x}_2 \in \mathbb{R}^3} & \quad \|\mathbf{x}_1 - \mathbf{x}_2\|^2 \\ \text{s.t.} & \quad A_1 \mathbf{x}_1 \leq \mathbf{b}_1 \\ & \quad A_2 \mathbf{x}_2 \leq \mathbf{b}_2. \end{aligned} \quad (2)$$

While many off-the-shelf solvers exist to solve QP problems, their performances scale poorly with respect to the number of constraints [42]. This is especially true in the presence of complex meshes composed of hundreds or thousands of vertices, for which QP solvers can take a few milliseconds to assess a collision, as we experimentally highlight in Sec. IV-C. Having established that solving collision detection requires dedicated methods, we turn our attention to solutions such as GJK, which has been shown to operate on a large class of shapes, ranging from simple primitives to very complex meshes.

**Recasting the distance computation problem onto the Minkowski difference.** The first important idea of 1988's paper by Gilbert, Johnson, and Keerthi [12] is to recast the distance computation problem onto the Minkowski difference  $\mathcal{D}$  of the shapes and defined as follows:

$$\mathcal{D} = \mathcal{A}_1 - \mathcal{A}_2 = \{\mathbf{x} = \mathbf{x}_1 - \mathbf{x}_2 \mid \mathbf{x}_1 \in \mathcal{A}_1, \mathbf{x}_2 \in \mathcal{A}_2\} \subset \mathcal{C}, \quad (3)$$

where  $\mathcal{C} = \mathbb{R}^n$  is the so-called *collision space*. The shapes  $\mathcal{A}_1$  and  $\mathcal{A}_2$  lie in the shape space and the Minkowski difference  $\mathcal{D}$  lies in the collision space.

Although both the shape space and the collision space are isomorphic to  $\mathbb{R}^n$ , we distinguish between the two to highlight the change in perspective. In Fig. 2, we illustrate the link between a pair of two convex shapes and their corresponding Minkowski difference. We stress that the Minkowski difference  $\mathcal{D}$  is *specific* to shapes  $\mathcal{A}_1$  and  $\mathcal{A}_2$ . If the relative position or relative orientation between  $\mathcal{A}_1$  and  $\mathcal{A}_2$  changes, their Minkowski difference changes accordingly.

The following properties, illustrated in Fig. 2, hold for the Minkowski difference  $\mathcal{D}$ :

- 1) Since  $\mathcal{A}_1$  and  $\mathcal{A}_2$  are convex sets,  $\mathcal{D}$  is also convex.
- 2) If  $\mathcal{A}_1$  and  $\mathcal{A}_2$  are intersecting, the origin of  $\mathcal{C}$ , denoted as  $\mathbf{0}_C$ , lies inside the Minkowski difference  $\mathcal{D}$ , *i.e.*  $\mathbf{0}_C = \mathbf{x}_1 - \mathbf{x}_2$  for some  $\mathbf{x}_1 \in \mathcal{A}_1$  and  $\mathbf{x}_2 \in \mathcal{A}_2$ .
- 3) If  $\mathcal{A}_1$  and  $\mathcal{A}_2$  are not intersecting, the projection of  $\mathbf{0}_C$  onto  $\mathcal{D}$ ,  $\mathbf{x}^* = \text{proj}_{\mathcal{D}}(\mathbf{0}_C)$ , corresponds to two vectors

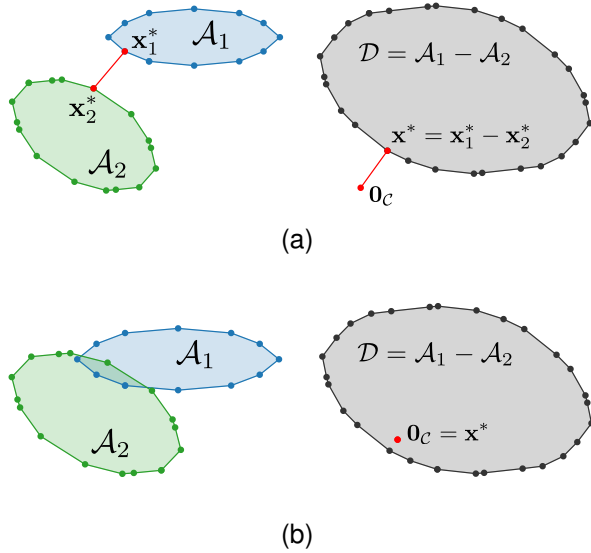


Fig. 2. (a) Distant vs. (b) overlapping pairs of shapes and their respective Minkowski difference. Left column: two convex shapes in 2D. Right column: the Minkowski difference  $\mathcal{D}$  of  $\mathcal{A}_1$  and  $\mathcal{A}_2$ . Since  $\mathcal{A}_1$  and  $\mathcal{A}_2$  are convex,  $\mathcal{D}$  is also convex. In (a), the shapes are not in collision hence the origin of the configuration space  $\mathcal{C}$ ,  $\mathbf{0}_{\mathcal{C}}$  (in red) lies outside the Minkowski difference,  $\mathbf{0}_{\mathcal{C}} \notin \mathcal{D}$ . The vector  $\mathbf{x}^* = \mathbf{x}_1^* - \mathbf{x}_2^*$  separates  $\mathcal{A}_1$  from  $\mathcal{A}_2$ . It is also equal to the projection of  $\mathbf{0}_{\mathcal{C}}$  onto the Minkowski difference  $\mathcal{D}$ ,  $\mathbf{x}^* = \text{proj}_{\mathcal{D}}(\mathbf{0}_{\mathcal{C}})$ . In (b), the shapes overlap, thus  $\mathbf{0}_{\mathcal{C}} \in \mathcal{D}$ . In this case, we have  $\mathbf{x}^* = \text{proj}_{\mathcal{D}}(\mathbf{0}_{\mathcal{C}}) = \mathbf{0}_{\mathcal{C}}$ .

1  $\mathbf{x}_1^* \in \mathcal{A}_1$  and  $\mathbf{x}_2^* \in \mathcal{A}_2$ , also called witness vectors in the  
 2 computational geometry literature [7]. Contrary to  $\mathbf{x}^*$ ,  
 3 these vectors  $\mathbf{x}_1^*$  and  $\mathbf{x}_2^*$  are not necessarily unique, as  
 4 is the case for non-strictly convex shapes such as two  
 5 parallel boxes.

6 4) Finally, we always have  $\|\mathbf{x}^*\| = \text{dist}(\mathcal{A}_1, \mathcal{A}_2)$ .

7 This final remark allows us to recast the distance computation  
 8 problem (1) onto the Minkowski difference as follows:

$$d_{1,2} = \min_{\mathbf{x} \in \mathcal{D}} \|\mathbf{x} - \mathbf{0}_{\mathcal{C}}\|^2 = \min_{\mathbf{x} \in \mathcal{D}} \|\mathbf{x}\|^2. \quad (4)$$

9 The convex optimization problem (4) is equivalent to (1)  
 10 and is known as a Minimum-Norm Point problem in the  
 11 optimization literature [34], [40], [43]. In our case,  $\mathbf{0}_{\mathcal{C}} \in \mathcal{C} = \mathbb{R}^n$   
 12 is the null vector *i.e.* the origin of the collision  
 13 space. We thus aim at finding the point in  $\mathcal{D}$  with the lowest  
 14 norm. This vector  $\mathbf{x}^*$  is the *optimal solution* to (4), given  
 15 by  $d_{1,2} = \|\mathbf{x}^*\|^2 = \text{dist}(\mathcal{A}_1, \mathcal{A}_2)^2$ .

16 Directly computing the Minkowski difference  $\mathcal{D}$  is neither  
 17 analytically tractable nor computationally efficient. Most of  
 18 the first and second-order methods for constrained convex  
 19 optimization problems, such as projected gradient descent or  
 20 interior point methods [44], are thus sub-optimal choices.  
 21 However, computing support vectors of the Minkowski differ-  
 22 ence  $\mathcal{D}$ , a notion defined hereinafter in this section, is relatively  
 23 simple and largely demonstrated by [12]. As we discuss next,  
 24 solving convex optimization problems by computing support  
 25 vectors is the strength of the Frank-Wolfe algorithm and its  
 26 variants [38].

27 **Distance computation using the Frank-Wolfe algorithm.**  
 28 The Frank-Wolfe algorithm (FW) [11] is one of the oldest

---

### Algorithm 1 Frank-Wolfe algorithm with linesearch [38]

---

Let  $\mathbf{x}_0 \in \mathcal{D}$ ,  $\epsilon > 0$

For  $k=0, 1, \dots$  do

- 1:  $\mathbf{d}_k = \nabla f(\mathbf{x}_k)$  ▷ Direction of support
  - 2:  $\mathbf{s}_k \in \arg \min_{\mathbf{s} \in \mathcal{D}} \langle \mathbf{d}_k, \mathbf{s} \rangle (= S_{\mathcal{D}}(\mathbf{d}_k))$  ▷ Support (8)
  - 3: **If**  $g_{FW}(\mathbf{x}_k) \leq \epsilon$ , **return**  $f(\mathbf{x}_k)$  ▷ Duality gap (16)
  - 4:  $\gamma_k = \arg \min_{\gamma \in [0,1]} f(\gamma \mathbf{x}_k + (1-\gamma)\mathbf{s}_k)$  ▷ Linesearch
  - 5:  $\mathbf{x}_{k+1} = \gamma_k \mathbf{x}_k + (1-\gamma_k)\mathbf{s}_k$  ▷ Update iterate  
*In the case of the distance computation problem (4),  
 where  $f(\mathbf{x}) = \|\mathbf{x}\|^2$ , line 4-5 correspond to projecting  $\mathbf{0}_{\mathcal{C}}$   
 on the segment  $[\mathbf{x}_k, \mathbf{s}_k]$ :*
  - 6:  $\mathbf{x}_{k+1} = \text{proj}_{[\mathbf{x}_k, \mathbf{s}_k]}(\mathbf{0}_{\mathcal{C}})$  ▷ Project  $\mathbf{0}_{\mathcal{C}}$  on  $[\mathbf{x}_k, \mathbf{s}_k]$
- 

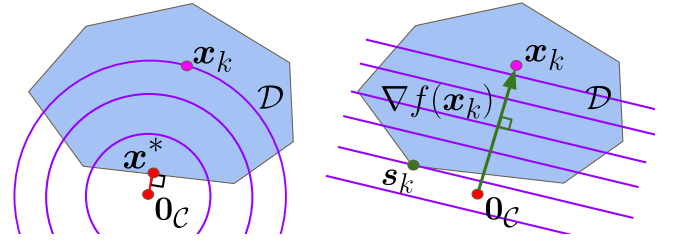


Fig. 3. Computing a support vector  $\mathbf{s}_k$  in direction  $\nabla f(\mathbf{x}_k)$  on convex set  $\mathcal{D}$ . We illustrate with the example of distance computation. On the left, we draw the Minkowski difference  $\mathcal{D}$  of which point of minimum norm (MNP) is  $\mathbf{x}^*$  *i.e.*  $\mathbf{x}^*$  is the projection of  $\mathbf{0}_{\mathcal{C}}$  onto  $\mathcal{D}$ ,  $\mathbf{x}^* = \text{proj}_{\mathcal{D}}(\mathbf{0}_{\mathcal{C}})$ . The iterate at iteration  $k$  of the FW algorithm is  $\mathbf{x}_k$ . In purple we draw the level sets of the function  $f(\mathbf{x}) = \|\mathbf{x}\|^2$ . On the right, we draw in purple the level sets of the linearization of  $f$  at iterate  $\mathbf{x}_k$ ,  $h_k$ . The first step of the FW algorithm is to compute support vector  $\mathbf{s}_k$  in the direction of  $\nabla f(\mathbf{x}_k)$  (green arrow),  $\mathbf{s}_k \in S_{\mathcal{D}}(\nabla f(\mathbf{x}_k))$ . In the second step of the FW algorithm, we compute  $\mathbf{x}_{k+1}$  as a convex combination of  $\mathbf{x}_k$  and  $\mathbf{s}_k$  *i.e.*  $\mathbf{x}_{k+1}$  is a point on the segment  $[\mathbf{x}_k, \mathbf{s}_k]$ .

convex optimization methods and solves the following con-  
 strained optimization problem:

$$f(\mathbf{x}^*) = \min_{\mathbf{x} \in \mathcal{D}} f(\mathbf{x}), \quad (5)$$

where  $f: \mathbb{R}^n \rightarrow \mathbb{R}$  is a convex and differentiable function and  
 $\mathcal{D}$  is a compact convex set. For our distance computation  
 problem (4), we use  $f(\mathbf{x}) = \|\mathbf{x}\|^2$  and the Minkowski  
 difference  $\mathcal{D}$  as convex constraint set. As a side note, the  
 following discussed algorithms all require an initial starting  
 point  $\mathbf{x}_0 \in \mathcal{D}$ . Shapes used in physics engines are usually  
 attached to a frame to keep track of their position and  
 orientation in space. We denote  $\mathbf{c}^1 \in \mathcal{A}_1$  and  $\mathbf{c}^2 \in \mathcal{A}_2$  the  
 origins of the frames attached to  $\mathcal{A}_1$  and  $\mathcal{A}_2$ , respectively. In  
 the rest of this paper, we take  $\mathbf{x}_0 = \mathbf{c}^1 - \mathbf{c}^2$ .

The FW algorithm, summarized in Alg. 1, is a gradient-  
 descent method. It consists in iteratively applying two steps in  
 order to converge towards the optimal solution  $\mathbf{x}^*$  of (5). If  
 we denote by  $\mathbf{x}_k$  the estimate of  $\mathbf{x}^*$  at iteration  $k$ , these two  
 steps correspond to:

- 1) First, we compute a support vector  $\mathbf{s}_k$  in the direction  
 of  $\nabla f(\mathbf{x}_k)$ , by solving a linear optimization problem  
 on  $\mathcal{D}$ .
- 2) Second, we update our current iterate  $\mathbf{x}_k$  to obtain  $\mathbf{x}_{k+1}$ ,  
 by taking a convex combination of the current iterate  $\mathbf{x}_k$   
 and the computed support vector  $\mathbf{s}_k$ .



In the following, we detail these steps in the context of distance computation. At iteration  $k$ , the current iterate  $\mathbf{x}_k$  is the estimate of the optimal solution  $\mathbf{x}^*$  and  $f(\mathbf{x}_k)$  is the estimate of the optimal value of (5),  $f(\mathbf{x}^*)$ , at iteration  $k$ . We write the linearization of the function  $f$  at  $\mathbf{x}_k$  and denote it as  $h_k$ :

$$h_k(\mathbf{s}) = f(\mathbf{x}_k) + \langle \nabla f(\mathbf{x}_k), \mathbf{s} - \mathbf{x}_k \rangle \quad (6)$$

where  $\mathbf{s}$  is a vector of  $\mathbb{R}^n$ ,  $\nabla f(\mathbf{x}_k)$  is the gradient of  $f$  at  $\mathbf{x}_k$  and  $\langle \cdot, \cdot \rangle$  denotes the dot product between two vectors of  $\mathbb{R}^n$ .

$\hookrightarrow$  **Step 1.** The first step of the FW algorithm at iteration  $k$  consists of finding a minimizer  $\mathbf{s}_k \in \mathcal{D}$  of  $h_k$  on the convex set  $\mathcal{D}$  (line 2 in Alg. 1). Such a vector  $\mathbf{s}_k$  is called a *support vector* of  $\mathcal{D}$  or simply a *support* and is defined as follows:

$$\mathbf{s}_k \in \arg \min_{\mathbf{s} \in \mathcal{D}} h_k(\mathbf{s}) = \arg \min_{\mathbf{s} \in \mathcal{D}} \langle \nabla f(\mathbf{x}_k), \mathbf{s} \rangle. \quad (7)$$

Fig. 3 gives a graphical understanding of support  $\mathbf{s}_k$ . The vector  $\mathbf{s}_k$  belongs to  $\mathcal{D}$  and is in the *most* opposite direction w.r.t.  $\nabla f(\mathbf{x}_k)$ . In order to highlight the importance of the direction in which a support  $\mathbf{s}_k$  is computed, we now introduce the notion of *support direction* and *support function*. Given a support direction  $\mathbf{d} \in \mathbb{R}^n$ , the support function  $S_{\mathcal{D}}$  returns a set of  $\mathcal{D}$  and is defined as:

$$S_{\mathcal{D}}(\mathbf{d}) = \arg \min_{\mathbf{s} \in \mathcal{D}} \langle \mathbf{d}, \mathbf{s} \rangle \subset \mathcal{D}. \quad (8)$$

The support function  $S_{\mathcal{D}}$  may return a set with more than one vector. We only need to use one vector of this set. Thinking in terms of the direction of support allows us to understand that this direction can be rescaled while preserving the output of the support function:

$$\forall \mathbf{d} \in \mathbb{R}^n, \forall \alpha > 0, S_{\mathcal{D}}(\alpha \mathbf{d}) = S_{\mathcal{D}}(\mathbf{d}). \quad (9)$$

A support  $\mathbf{s}_k \in \mathcal{D}$  at iteration  $k$  is thus computed in the direction  $\mathbf{d}_k = \nabla f(\mathbf{x}_k)$  and belongs to  $S_{\mathcal{D}}(\nabla f(\mathbf{x}_k))$ ,  $\mathbf{s}_k \in S_{\mathcal{D}}(\nabla f(\mathbf{x}_k))$ .

We now explain how to compute the support vector  $\mathbf{s}_k$  in the case of the distance computation problem (4) where we minimize  $f(\mathbf{x}) = \|\mathbf{x}\|^2$  on the Minkowski difference  $\mathcal{D}$  of  $\mathcal{A}_1$  and  $\mathcal{A}_2$ . First, we have  $\nabla f(\mathbf{x}) = 2\mathbf{x}$ . Therefore, in the case of problem (4), it follows that:

$$\mathbf{s}_k \in S_{\mathcal{D}}(\mathbf{x}_k) = \arg \min_{\mathbf{s} \in \mathcal{D}} \langle \mathbf{x}_k, \mathbf{s} \rangle. \quad (10)$$

As demonstrated by [12], any vector  $\mathbf{s} \in S_{\mathcal{D}}(\mathbf{d})$  related to the Minkowski difference can be decomposed as the difference between two support vectors  $\mathbf{s}_{\mathcal{A}_1} \in S_{\mathcal{A}_1}(\mathbf{d})$  and  $\mathbf{s}_{\mathcal{A}_2} \in S_{\mathcal{A}_2}(-\mathbf{d})$  over the two individual shapes, leading to the following relation:

$$\mathbf{s} = \mathbf{s}_{\mathcal{A}_1} - \mathbf{s}_{\mathcal{A}_2} \in S_{\mathcal{D}}(\mathbf{d}). \quad (11)$$

Equation (11) shows that we can construct a support of the Minkowski difference from the supports of the original shapes. This property highlights the powerful change of perspective of working on the Minkowski difference. Indeed, there exists a large number of shapes for which computing supports is simple: spheres, ellipsoids, cylinders, capsules, polytopes etc. [7], [21], [26]. Fig. 4 illustrates the construction of a support of the Minkowski difference  $\mathcal{D}$  using the supports of the original shapes  $\mathcal{A}_1$  and  $\mathcal{A}_2$ .

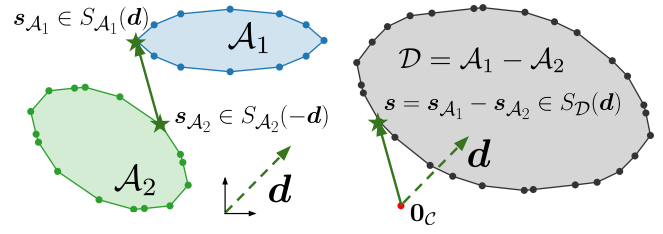


Fig. 4. Computing a support vector on the Minkowski difference using support vectors (represented by star shapes in the drawing) on the individual shapes. The vector  $\mathbf{s}_{\mathcal{A}_1}$  is a support vector of shape  $\mathcal{A}_1$  in direction  $\mathbf{d}$ . The vector  $\mathbf{s}_{\mathcal{A}_2}$  is a support vector of shape  $\mathcal{A}_2$  in direction  $-\mathbf{d}$ . The constructed vector  $\mathbf{s} = \mathbf{s}_{\mathcal{A}_1} - \mathbf{s}_{\mathcal{A}_2}$  is a support vector of the Minkowski difference  $\mathcal{D}$  in the direction  $\mathbf{d}$ .

$\hookrightarrow$  **Step 2.** Once a support vector  $\mathbf{s}_k \in S_{\mathcal{D}}(\mathbf{x}_k)$  has been computed, we update the iterate  $\mathbf{x}_k$  to obtain  $\mathbf{x}_{k+1}$  by taking a convex combination between  $\mathbf{s}_k$  and  $\mathbf{x}_k$ . The original FW algorithm uses a parameter-free update:

$$\mathbf{x}_{k+1} = \gamma_k \mathbf{x}_k + (1 - \gamma_k) \mathbf{s}_k, \quad (12)$$

where  $\gamma_k = \frac{k+1}{k+2} \in [0, 1]$  controls the step size. Alternatively, a line search can be carried out to find a better iterate  $\mathbf{x}_{k+1}$  (line 4 in Alg. 1):

$$\begin{aligned} \gamma_k &= \arg \min_{\gamma \in [0, 1]} f(\gamma \mathbf{x}_k + (1 - \gamma) \mathbf{s}_k) \\ \mathbf{x}_{k+1} &= \gamma_k \mathbf{x}_k + (1 - \gamma_k) \mathbf{s}_k. \end{aligned} \quad (13)$$

In the distance computation case where  $f(\mathbf{x}) = \|\mathbf{x}\|^2$ , this linesearch (13) is equivalent to projecting  $\mathbf{0}_C$  onto the segment  $[\mathbf{x}_k, \mathbf{s}_k]$ ,  $\mathbf{x}_k = \text{proj}_{[\mathbf{x}_k, \mathbf{s}_k]}(\mathbf{0}_C)$  (line 4 in Alg. 1). Since  $\mathcal{D}$  is convex, both (12) and (13) updates are guaranteed to remain in  $\mathcal{D}$ .

**Stopping criteria.** As Frank-Wolfe deals with convex problems, the *duality gap* associated with problem (5) can be used as a stopping criterion. Due to its convexity, the function  $f$  is always above its linearization. Otherwise said, for any  $\mathbf{x} \in \mathbb{R}^n$  and any  $\mathbf{s} \in \mathbb{R}^n$ :

$$f(\mathbf{s}) \geq f(\mathbf{x}) + \langle \nabla f(\mathbf{x}), \mathbf{s} - \mathbf{x} \rangle. \quad (14)$$

Reworking this inequality and applying the min operator enables us to compute the Frank-Wolfe duality gap  $g_{\text{FW}}(\mathbf{x}) \in \mathbb{R}_+$  which gives an upper-bound on the difference  $f(\mathbf{x}) - f(\mathbf{x}^*)$ :

$$f(\mathbf{x}) - f(\mathbf{x}^*) \leq -\min_{\mathbf{s} \in \mathcal{D}} \langle \nabla f(\mathbf{x}), \mathbf{s} - \mathbf{x} \rangle = g_{\text{FW}}(\mathbf{x}). \quad (15)$$

In particular, at iteration  $k$  of the FW algorithm, we have:

$$f(\mathbf{x}_k) - f(\mathbf{x}^*) \leq g_{\text{FW}}(\mathbf{x}_k) = \langle \nabla f(\mathbf{x}_k), \mathbf{x}_k - \mathbf{s}_k \rangle, \quad (16)$$

where  $\mathbf{s}_k \in S_{\mathcal{D}}(\nabla f(\mathbf{x}_k))$  is the support vector computed at iteration  $k$  in the direction of  $\nabla f(\mathbf{x}_k)$ . The duality-gap  $g_{\text{FW}}(\mathbf{x}_k)$  serves as a convergence criterion for the Frank-Wolfe method and is cheap to compute. Applied to the distance computation problem (4), the duality gap at iteration  $k$ ,  $g_{\text{FW}}(\mathbf{x}_k)$ , guarantees that:

$$\|\mathbf{x}_k\|^2 - \|\mathbf{x}^*\|^2 \leq g_{\text{FW}}(\mathbf{x}_k) = 2\langle \mathbf{x}_k, \mathbf{x}_k - \mathbf{s}_k \rangle. \quad (17)$$

**Algorithm 2** Boolean collision checking: separating plane condition

---

Insert after line 2 in Alg. 1:

1: **If**  $\max(0, \langle \mathbf{d}_k / \|\mathbf{d}_k\|, \mathbf{s}_k \rangle) > \epsilon_{\text{col}}$ , **return False**  
**If after termination**  $d_{1,2} \leq \epsilon_{\text{col}}$ , **return True, otherwise return False.**

---

1 Using the triangular inequality of the Euclidian norm and the  
2 convexity of the Minkowski difference  $\mathcal{D}$ , we can show that:

$$\|\mathbf{x}_k - \mathbf{x}^*\|^2 \leq \|\mathbf{x}_k\|^2 - \|\mathbf{x}^*\|^2 \leq g_{\text{FW}}(\mathbf{x}_k). \quad (18)$$

3 Inequality (18) is useful in practice as it allows the fine  
4 control of the desired tolerance on the distance to the optimal  
5 solution  $\mathbf{x}^*$  (line 3 in Alg. 1). Indeed, if ones wants to compute  
6 an estimate  $\mathbf{x}$  of the optimal solution  $\mathbf{x}^*$  at precision  $\epsilon$ ,  
7 meaning that  $\|\mathbf{x} - \mathbf{x}^*\| \leq \sqrt{\epsilon}$ , it is sufficient to check that  
8  $g_{\text{FW}}(\mathbf{x}) \leq \epsilon$ .

9 **Boolean collision checking.** As mentioned earlier, the problem  
10 of distance computation encompasses the problem of  
11 collision checking. Indeed, in collision checking, we are only  
12 interested in finding a separating plane between  $\mathcal{A}_1$  and  $\mathcal{A}_2$ ,  
13 if it exists. This is equivalent to finding a separating plane  
14 between  $\mathcal{D}$  and  $\mathbf{0}_C$ . For *any* support direction  $\mathbf{d}$ , if we have:

$$\langle \mathbf{d}, \mathbf{s} \rangle > 0, \mathbf{s} \in S_{\mathcal{D}}(\mathbf{d}), \quad (19)$$

15 then the plane supported by the vector  $\mathbf{d}$  separates  $\mathcal{D}$   
16 from  $\mathbf{0}_C$  [21]. This also means that, in the case where the  
17 two shapes intersect, collision checking has the same com-  
18 putational complexity as distance computation. In general, at  
19 iteration  $k$ , the value  $\max(0, \langle \mathbf{d}_k / \|\mathbf{d}_k\|, \mathbf{s}_k \rangle)$  is a lower bound  
20 on the distance between the shapes,  $\text{dist}(\mathcal{A}_1, \mathcal{A}_2)$ , and it can  
21 be used as a stopping criterion in the boolean collision check.  
22 As soon as the lower bound on  $\text{dist}(\mathcal{A}_1, \mathcal{A}_2)$  is guaranteed  
23 to be positive, the algorithm can be stopped. Otherwise, the  
24 algorithm continues until the stopping criterion defined by (18)  
25 is met. As shown in Alg. 2, we add this separating plane  
26 condition before line 2 in Alg. 1. The condition on the lower  
27 bound of  $\text{dist}(\mathcal{A}_1, \mathcal{A}_2)$  is met relative to a threshold  $\epsilon_{\text{col}}$ . This  
28 threshold sets at what distance the shapes are considered to  
29 be in collision and depends on the application. In practice,  
30 since we use double-precision floats in our benchmarks (see  
31 Sec. IV), the test on the lower bound of  $\text{dist}(\mathcal{A}_1, \mathcal{A}_2)$  can be  
32 computed down to machine precision. This means the distance  
33 computation threshold  $\epsilon$  can take values down to  $10^{-12}$  in (18).  
34 This corresponds to a precision on the distance between shapes  
35 on the order of micro-meters ( $\sqrt{\epsilon} = 10^{-6}\text{m}$ ). In robotics  
36 applications where the entire pipeline is no more precise than  
37 millimeters, it is often sufficient to consider that below a  
38 threshold of  $10^{-4}\text{m}$  (i.e  $\epsilon = 10^{-8}$ ) the shapes are in collision;  
39 above that threshold the shapes are not in collision. In our  
40 applications, we use  $\epsilon_{\text{col}} = \sqrt{\epsilon}$ .

42 **Computing support vector on meshes.** While the support  
43 vector of basic primitives (sphere, ellipsoid, box, etc.) presents  
44 closed-form solutions, this is not the case for meshes. In the  
45 case of convex meshes, an efficient approach for computing the

**Algorithm 3** Frank-Wolfe algorithm with line-search (see Alg. 1) rewritten with active-sets and applied to the distance computation problem (4)

---

Let  $\mathbf{x}_0 \in \mathcal{D}$ ,  $W_0 = \{\mathbf{x}_0\}$ ,  $\epsilon > 0$ 

For  $k=0, 1, \dots$  **do**

- 1:  $\mathbf{d}_k = \mathbf{x}_k$  ▷ Direction of support
  - 2:  $\mathbf{s}_k \in S_{\mathcal{D}}(\mathbf{d}_k)$  ▷ Support (8)
  - 3: **If**  $g_{\text{FW}}(\mathbf{x}_k) \leq \epsilon$ , **return**  $f(\mathbf{x}_k)$  ▷ Duality gap (16)
  - 4:  $\widetilde{W}_{k+1} = W_k \cup \{\mathbf{s}_k\}$  ▷ Augment active-set
  - 5:  $\mathbf{x}_{k+1} = \text{proj}_{\text{conv}(\widetilde{W}_{k+1})}(\mathbf{0}_C)$  ▷ Project  $\mathbf{0}_C$  on  $\text{conv}(\widetilde{W}_{k+1})$
  - 6:  $W_{k+1} = \{\mathbf{x}_{k+1}\}$  ▷ Update active-set
- 

support direction of meshes is the *hill-climbing* algorithm [26],  
which allows retrieving the supporting vertex or face of the  
meshes thanks to a simple neighbor-descent procedure. Yet,  
this procedure is sensitive to the initial-guess solution. By  
leveraging Nesterov and Polyak acceleration schemes intro-  
duced in Sec. III, which both tend to reduce the oscillations  
hindered by gradient-descent type algorithms, we show in  
Sec. IV that this helps the hill-climbing algorithm to perform  
less iterations in practice, leading to faster computation times.

**The Frank-Wolfe active-set.** As with many gradient-descent  
algorithms, the FW method tends to zig-zag towards the  
optimal solution [40], slowing down the convergence to the  
optimum. This behavior is undesired and amplified if the  
optimal solution  $\mathbf{x}^*$  lies close to the boundary of the constraint  
set  $\mathcal{D}$ . In collision detection, this corresponds to the case  
where the two shapes are not intersecting. This zig-zagging  
behavior is due to the way that Frank-Wolfe approaches the  
set of active constraints [40], also called *active-set* in the  
optimization literature [44]. In the FW setting, the active set  
at iteration  $k$ , denoted  $W_k = \{\mathbf{s}^0, \dots, \mathbf{s}^r\} \subset \mathcal{D}$ , is the set  
of vectors in  $\mathcal{D}$  used by the algorithm to maintain a convex  
combination of the iterate  $\mathbf{x}_k$ :

$$\mathbf{x}_k = \sum_{i=0}^r \lambda^i \mathbf{s}^i, \sum_{i=0}^r \lambda^i = 1 \text{ with } \mathbf{s}^i \in W_k \subset \mathcal{D} \text{ and } \lambda^i > 0. \quad (20)$$

In Alg. 3, we rewrite the FW algorithm with line search  
(Alg. 1) in order to highlight the notion of active set:

- At iteration  $k$ , the active-set is only composed  
of  $\mathbf{x}_k$ ,  $W_k = \{\mathbf{x}_k\}$ .
- The active-set  $W_k$  is then augmented by computing a  
support  $\mathbf{s}_k$  (line 2 in Alg. 3) to obtain  $\widetilde{W}_{k+1} = \{\mathbf{x}_k, \mathbf{s}_k\}$   
(line 4 in Alg. 3).
- We then minimize function  $f$  on the convex-hull  
of  $\widetilde{W}_{k+1}$ ,  $\text{conv}(\widetilde{W}_{k+1})$ , which is simply the seg-  
ment  $[\mathbf{x}_k, \mathbf{s}_k]$ . For the distance computation problem (4),  
this linesearch operation is equivalent to projecting  $\mathbf{0}_C$   
onto the segment  $[\mathbf{x}_k, \mathbf{s}_k]$  (line 5 in Alg. 3).
- Finally, the active-set is updated  $W_{k+1} = \{\mathbf{x}_{k+1}\}$  (line 6  
in Alg. 3).

In practice, discarding previously computed supports when  
updating the active set is inefficient and causes the zig-  
zagging phenomenon observed in the FW algorithm [40]. In  
the optimization literature, a rich and wide variety of variants

1 of the FW algorithm have been introduced to efficiently cope  
 2 with the active set in order to improve the convergence rate  
 3 of the FW method [34], [36], [37], [45], [46]. However,  
 4 these variants remain too generic and are not suited for the  
 5 specific problem of collision detection. In the following, we  
 6 propose instead incorporating the active-set strategy used in  
 7 GJK within the Frank-Wolfe setting.

8 **Connection between GJK and Frank-Wolfe.** In the case  
 9 of collision detection, [12] developed an efficient strategy to  
 10 handle the active set at a minimal cost. To represent the current  
 11 estimate  $\mathbf{x}_k$  and the optimal solution  $\mathbf{x}^*$ , GJK exploits the  
 12 concept of *simplexes* in  $\mathbb{R}^3$ . A simplex in  $\mathbb{R}^n$  corresponds to  
 13 a set containing *at most*  $n + 1$  vectors of  $\mathbb{R}^n$ , and the *rank*  $r$   
 14 of a simplex is the number of vectors it contains ( $0 < r \leq$   
 15  $n + 1$ ). For 3-dimensional spaces, a simplex corresponds either  
 16 to a point ( $r = 1$ ), a segment ( $r = 2$ ), a triangle ( $r = 3$ ),  
 17 or a tetrahedron ( $r = 4$ ). Similarly to the simplex methods  
 18 for Linear Programming [47], the Carathéodory theorem [48]  
 19 motivates the use of simplexes. Let  $\mathcal{Y}$  be a set of  $N \geq n$   
 20 vectors in  $\mathbb{R}^n$ ,  $\mathcal{Y} = \{\mathbf{y}^i \in \mathbb{R}^n\}_{0 \leq i \leq N}$ . The Carathéodory  
 21 theorem states that any vector  $\mathbf{x} \in \text{conv}(\mathcal{Y})$  can be expressed  
 22 as the convex combination of at most  $n + 1$  vectors of  $\mathcal{Y}$ :

$$\mathbf{x} = \sum_{j=0}^r \lambda^j \mathbf{y}^j, \text{ with } \mathbf{y}^j \in \mathcal{Y}, \lambda^j > 0, \sum_{i=0}^r \lambda^i = 1. \quad (21)$$

23 Hence, any vector in  $\mathcal{D}$ , and particularly the optimal solu-  
 24 tion  $\mathbf{x}^* \in \mathcal{D} = \text{conv}(\mathcal{D})$  of the distance computation  
 25 problem (4), can be identified as a convex combination of  
 26 the vectors composing a simplex  $W$ . Relying on simplexes  
 27 is attractive as there is no need to run any algorithm to  
 28 compute the convex hull of a simplex as they are convex  
 29 by construction. Frank-Wolfe algorithms may operate on more  
 30 complex active sets, which might become hard to tackle from  
 31 a computational point of view [38], [40]. In other words, the  
 32 problem of finding the optimal solution  $\mathbf{x}^*$  can be reformulated  
 33 as the problem of identifying the optimal simplex  $W^*$  on  
 34 which  $\mathbf{x}^*$  can be decomposed into a convex combination. This  
 35 is precisely the approach followed by GJK that we now detail  
 36 as well as illustrate in Fig. 5.

37 At iteration  $k$  of GJK, the current iterate  $\mathbf{x}_k$  is a convex  
 38 combination of the vectors composing the simplex  $W_k$  of  
 39 rank  $r_k \leq n$ . This corresponds to Fig. 5a. To update  $\mathbf{x}_k$   
 40 and  $W_k$ , the following procedure is applied:

- 41 • After computing support vector  $\mathbf{s}_k$  (line 2 in Alg. 3,  
 42 illustrated in Fig. 5b), we add  $\mathbf{s}_k$  to  $W_k$  to ob-  
 43 tain  $\widetilde{W}_{k+1} = W_k \cup \{\mathbf{s}_k\}$  (line 4 in Alg. 3). The set  $\widetilde{W}_{k+1}$   
 44 is now a simplex of rank  $\widetilde{r}_{k+1} \leq n + 1$ , as shown in  
 45 Fig. 5c.
- 46 • We then minimize function  $f(\mathbf{x}) = \|\mathbf{x}\|^2$  on  $\widetilde{W}_{k+1}$   
 47 to obtain  $\mathbf{x}_{k+1}$ , corresponding to projecting  $\mathbf{0}_C$   
 48 onto  $\widetilde{W}_{k+1}$ :  $\mathbf{x}_{k+1} = \text{proj}_{\text{conv}(\widetilde{W}_{k+1})}(\mathbf{0}_C)$ <sup>1</sup> (line 5 in  
 49 Alg. 3). This projection is illustrated in figures 5c and 5d.
- 50 • We then have two cases, summarized in Alg 4:

<sup>1</sup>The efficient projection onto simplexes in  $\mathbb{R}^3$ , named the *distance sub-  
 algorithm* by [12], is thoroughly covered in [7], [21] and its robustness is  
 improved in [30].

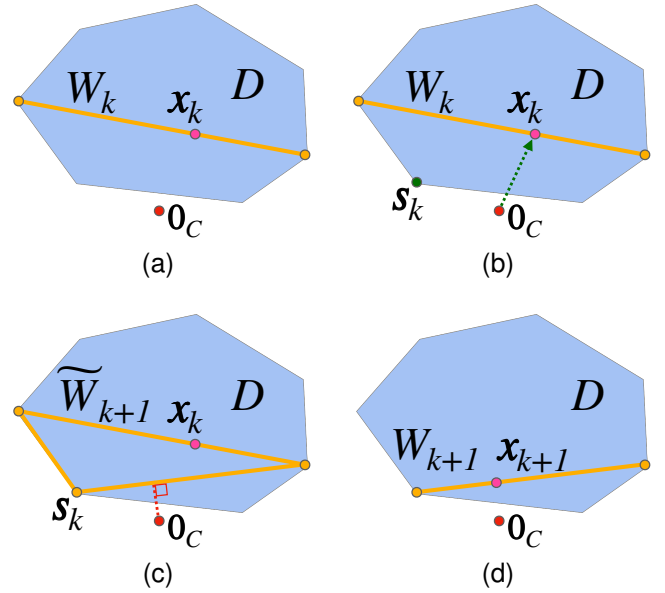


Fig. 5. Illustration of the GJK simplex strategy in 2D: (a) beginning of the  $k^{\text{th}}$  iteration, (b) support point computation, (c) simplex augmentation, (d) simplex update.

- 1) If  $\mathbf{x}_{k+1} = \mathbf{0}_C$ , the algorithm is stopped. Thus, we have  $\mathbf{x}^* = \mathbf{0}_C$  and  $d_{1,2} = 0$  in (4) (line 1 in Alg. 4).
- 2) Otherwise, we construct  $W_{k+1}$  from  $\widetilde{W}_{k+1}$ . To do so, we retain only the minimal number of vectors in  $\widetilde{W}_{k+1}$  needed to express  $\mathbf{x}_{k+1}$  as a convex combination (line 2 in Alg. 4). Indeed, as  $\mathbf{0}_C \notin \widetilde{W}_{k+1}$ , the projection  $\mathbf{x}_{k+1}$  of  $\mathbf{0}_C$  on  $\widetilde{W}_{k+1}$  necessarily lies on a face of  $\widetilde{W}_{k+1}$ , and can be expressed as a convex combination of the vectors composing this face. This ensures that  $W_{k+1}$  is necessarily of rank  $r_{k+1} < \widetilde{r}_{k+1} \leq n + 1$ . For example, Fig. 5d shows the result of the simplex update obtained in Fig. 5c.

Through this discussion, it is clear that GJK is a particular case of Frank-Wolfe. More specifically, it is a sub-case of the fully-corrective Frank-Wolfe algorithm analyzed by [40]. The strategy used by GJK to handle the active set has proved to be very efficient in practice and renders the GJK algorithm state-of-the-art for collision detection. In the next section, we propose to leverage the formulation of collision detection as a Frank-Wolfe sub-case to accelerate its convergence following the well-established Polyak and Nesterov acceleration paradigm [41].

### III. ACCELERATING COLLISION DETECTION

Gradient descent (GD) is the backbone of many convex optimization methods and relies solely on the gradient of the objective function. Second-order methods [44], such as Newton methods, have faster convergence rates than GD at the price of requiring the computation and the inversion of Hessian quantities. Momentum methods have thus been introduced in the optimization literature to provide gradient-based methods with improved convergence rates without requiring



**Algorithm 4** Fully-corrective FW using simplexes, applied to the distance computation problem (4). This algorithm is identical to GJK [12]

In Alg. 3, let  $W_0 = \emptyset$  and replace line 6 by:

1: **If**  $\mathbf{x}_{k+1} = \mathbf{0}_c$ , **return** 0

If the algorithm has not terminated, update  $\widetilde{W}_{k+1}$  to retain only the smallest number of vectors needed to express  $\mathbf{x}_{k+1}$ :

2:  $W_{k+1} = \{\mathbf{s}^1, \dots, \mathbf{s}^r\}$  where  $\mathbf{s}^1, \dots, \mathbf{s}^r$  are the smallest number of vectors in  $\widetilde{W}_{k+1}$  such that  $\mathbf{x}_{k+1}$  is a convex combination of  $\mathbf{s}^1, \dots, \mathbf{s}^r$ .

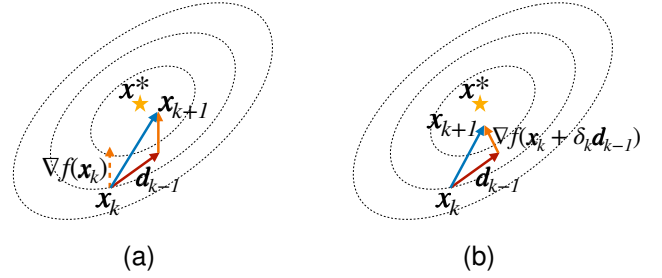


Fig. 6. (a) Polyak and (b) Nesterov acceleration schemes for unconstrained gradient descent. The gradient descent algorithm aims at finding the optimum  $\mathbf{x}^*$  by following the slope given by the gradient of function  $f$ ,  $\nabla f$ . The vector  $\mathbf{d}_{k-1}$  is the momentum accumulated over the optimization trajectory. The two schemes differ in where the gradient is computed at iteration  $k$ ; the Nesterov scheme introduces an intermediary point  $\mathbf{y}_k = \mathbf{x}_k + \delta_k \mathbf{d}_{k-1}$  to compute the gradient.

1 costly Hessian evaluation. In this section, we use recent  
2 work linking the *Polyak* and *Nesterov* accelerations of GD  
3 to the FW algorithm [13], [14] to globally accelerate collision  
4 detection. These global accelerations of collision detection are  
5 experimentally evaluated in Sec. IV on several benchmarks.

6 *A. Background on acceleration methods in convex optimization*

8 **Polyak acceleration for unconstrained optimization.** We  
9 initially consider the following *unconstrained* minimization  
10 problem:

$$f(\mathbf{x}^*) = \min_{\mathbf{x} \in \mathbb{R}^n} f(\mathbf{x}), \quad (22)$$

11 where  $f : \mathbb{R}^n \rightarrow \mathbb{R}$  is a convex and differentiable function. The  
12 vanilla gradient-descent algorithm follows the slope of  $f$  given  
13 by its gradient  $\nabla f$ . The following scheme is applied iteratively  
14 until a given convergence criterion is met (e.g.,  $\|\nabla f(\mathbf{x}_k)\| <$   
15  $\epsilon$ , with  $\epsilon$  being the desired precision):

$$\mathbf{x}_{k+1} = \mathbf{x}_k + \alpha_k \nabla f(\mathbf{x}_k), \quad (23)$$

16 where  $\mathbf{x}_k \in \mathbb{R}^n$  is the current iterate and  $\alpha_k \in \mathbb{R}$  is  
17 the gradient step. This standard setting leads to a simple  
18 implementation with linear convergence rate ( $O(1/k)$ ).

To go beyond this linear convergence regime, acceleration techniques have been devised in the optimization community to provide quadratic convergence rate ( $O(1/k^2)$ ) or more [35], by relying on relatively cheap gradient evaluations. Among these gradient-descent acceleration techniques, the Polyak (or Heavy-Ball) [49] and Nesterov acceleration [41] are two of the better-studied and most popular in practice [35]. These techniques are based on accumulating previously computed gradients in a *momentum* term  $\mathbf{d}_k$  and using this momentum  $\mathbf{d}_k$  to update the current iterate  $\mathbf{x}_k$ . The Polyak update scheme for unconstrained gradient descent is illustrated in Fig. 6a and goes as follows:

$$\mathbf{d}_k = \delta_k \mathbf{d}_{k-1} + \alpha_k \nabla f(\mathbf{x}_k) \quad (24a)$$

$$\mathbf{x}_{k+1} = \mathbf{x}_k + \mathbf{d}_k, \quad (24b)$$

19 where schemes  $\delta_k \in \mathbb{R}$  is the momentum parameter. The  
20 role of momentum  $\mathbf{d}_k$  is to smooth the trajectory of iterates  
21 converging towards the optimum by geometrically averaging  
22 previously computed gradients. The  $\delta_k$  momentum parameter  
23 is selected to prevent damping or overshooting of the iterate  
24 trajectory when going towards the optimal solution  $\mathbf{x}^*$ .

**Nesterov acceleration for unconstrained optimization.** The Nesterov update scheme is the second most well-known method for accelerating unconstrained gradient descent and it is only a slight modification on top of the Polyak scheme. Contrary to the Polyak case, in the Nesterov acceleration scheme the current iterate  $\mathbf{x}_k$  is extrapolated using the momentum term  $\mathbf{d}_k$  to compute the intermediate vector  $\mathbf{y}_k = \mathbf{x}_k + \delta_k \mathbf{d}_k$ . The gradient is then computed at the vector  $\mathbf{y}_k$ . The Nesterov update scheme for unconstrained gradient descent is illustrated in Fig. 6b and goes as:

$$\mathbf{y}_k = \mathbf{x}_k + \delta_k \mathbf{d}_{k-1} \quad (25a)$$

$$\mathbf{d}_k = \delta_k \mathbf{d}_{k-1} + \alpha_k \nabla f(\mathbf{y}_k) \quad (25b)$$

$$\mathbf{x}_{k+1} = \mathbf{x}_k + \mathbf{d}_k \quad (25c)$$

where  $\delta_k$  is the momentum parameter as in the Polyak scheme, and  $\mathbf{y}_k \in \mathbb{R}^n$  is an intermediate quantity. Computing the term  $\mathbf{y}_k$  leads to an anticipatory behavior in similar spirit to extra-gradient methods [35].

**Accelerating the Frank-Wolfe algorithm with Polyak and Nesterov.** Recent works of [13], [14] have proposed to adapt the Polyak and Nesterov accelerations to the FW setting. We propose to leverage and adapt this FW acceleration scheme to the context of collision detection, by notably extending the FW formulation of collision detection previously developed in Sec. II.

In the original FW algorithm, the support vector at iteration  $k$ ,  $\mathbf{s}_k$ , is computed in the direction of the gradient  $\nabla f(\mathbf{x}_k)$  (line 1 in Alg. 1). In the Polyak acceleration of FW proposed by [13], the direction of support for computing  $\mathbf{s}_k$  is instead defined by:

$$\mathbf{d}_k = \delta_k \mathbf{d}_{k-1} + (1 - \delta_k) \nabla f(\mathbf{x}_k) \quad (26a)$$

$$\mathbf{s}_k = S_{\mathcal{D}}(\mathbf{d}_k), \quad (26b)$$

where  $\delta_k = \frac{k+1}{k+3} \in [0, 1]$  is the momentum parameter and  $S_{\mathcal{D}}$  is the support function as defined in (8). In the Nesterov acceleration of FW proposed by [14], the direction of support for computing  $\mathbf{s}_k$  is slightly different from the Polyak scheme (26) as it introduces  $\mathbf{y}_k$ , an intermediary vector as in the GD Nesterov scheme (25) in order to evaluate the

**Algorithm 5** Polyak-accelerated and Nesterov-accelerated Frank-Wolfe [13], [14]

In Alg. 1 and Alg. 3, let  $\mathbf{d}_{-1} = \mathbf{s}_{-1} = \mathbf{x}_0$ ,  $\delta_k = \frac{k+1}{k+3}$  and replace line 1 by:

$$\begin{aligned} 1: \mathbf{y}_k &= \begin{cases} \mathbf{x}_k & \text{Polyak} \\ \delta_k \mathbf{x}_k + (1 - \delta_k) \mathbf{s}_{k-1} & \text{Nesterov} \end{cases} \\ 2: \mathbf{d}_k &= \delta_k \mathbf{d}_{k-1} + (1 - \delta_k) \nabla f(\mathbf{y}_k) \end{aligned}$$

gradient  $\nabla f(\mathbf{y}_k)$ :

$$\mathbf{y}_k = \delta_k \mathbf{x}_k + (1 - \delta_k) \mathbf{s}_{k-1} \quad (27a)$$

$$\mathbf{d}_k = \delta_k \mathbf{d}_{k-1} + (1 - \delta_k) \nabla f(\mathbf{y}_k) \quad (27b)$$

$$\mathbf{s}_k = S_{\mathcal{D}}(\mathbf{d}_k), \quad (27c)$$

1 where  $\mathbf{s}_{k-1}$  is the support vector computed at the previous  
2 iteration. To ensure  $\mathbf{y}_k$  stays in  $\mathcal{D}$ , it is a convex combination  
3 of  $\mathbf{x}_k$  and  $\mathbf{s}_{k-1}$ , both vectors of  $\mathcal{D}$ . The direction of support is  
4 then obtained by taking a convex combination of the previous  
5 support direction  $\mathbf{d}_{k-1}$  and the gradient  $\nabla f(\mathbf{y}_k)$ . Both the  
6 Polyak and Nesterov accelerations of Frank-Wolfe are summed  
7 up in Alg. 5.

8 The works [13], [14] have experimentally shown that these  
9 accelerations strategies lead to a better convergence rate of the  
10 FW algorithm when compared to the original FW algorithm.  
11 In the following, we explain how to adapt the Polyak and  
12 Nesterov accelerations of FW to collision detection.

13 *B. Acceleration of collision detection and distance computa-*  
14 *tion*

**Adapting Nesterov and Polyak fully-corrective Frank-Wolfe to distance computation.** Preserving GJK's simplex strategy is crucial for collision detection as it greatly speeds up the vanilla FW algorithm. Therefore, we adapt (26) and (27) accordingly as:

$$\mathbf{y}_k = \begin{cases} \mathbf{x}_k & \text{if Polyak} \\ \delta_k \mathbf{x}_k + (1 - \delta_k) \mathbf{s}_{k-1} & \text{if Nesterov} \end{cases} \quad (28a)$$

$$\mathbf{d}_k = \delta_k \mathbf{d}_{k-1} + (1 - \delta_k) \nabla f(\mathbf{y}_k) \quad (28b)$$

$$\mathbf{s}_k = S_{\mathcal{D}}(\mathbf{d}_k), \quad (28c)$$

$$\widetilde{W}_{k+1} = W_k \cup \{\mathbf{s}_k\}, \quad (28d)$$

$$\mathbf{x}_{k+1} = \text{proj}_{\text{conv}(\widetilde{W}_{k+1})}(\mathbf{0}_{\mathcal{C}}). \quad (28e)$$

These steps are also summarized in Alg. 6. The update of simplex  $W_{k+1}$  from  $\widetilde{W}_{k+1}$  is then identical to the one described in Alg. 4. The original duality gap defined in Sec. II (Eq. 16) can no longer be used as a convergence criterion. Indeed, the following inequality:

$$\|\mathbf{x}_k - \mathbf{x}^*\|^2 \leq g_{\text{FW}}(\mathbf{x}_k) = 2\langle \mathbf{x}_k, \mathbf{x}_k - \mathbf{s}_k \rangle, \quad \mathbf{s}_k \in S_{\mathcal{D}}(\mathbf{x}_k),$$

15 is no longer valid because the support vector  $\mathbf{s}_k$  is no longer  
16 computed in the direction of the gradient  $\nabla f(\mathbf{x}_k) = 2\mathbf{x}_k$ .  
17 Next we will show that the original stopping criterion devised  
18 in Sec. II cannot be used and we need to derive a new one.

**Algorithm 6** Polyak and Nesterov-accelerated GJK

Let  $\mathbf{x}_0 \in \mathcal{D}$ ,  $W_0 = \emptyset$ ,  $\mathbf{d}_{-1} = \mathbf{s}_{-1} = \mathbf{x}_0$ ,  $\epsilon > 0$

For  $k=0, 1, \dots$  do

$$1: \delta_k = \frac{k+1}{k+3} \quad \triangleright \text{Momentum parameter value}$$

$$2: \mathbf{y}_k = \begin{cases} \mathbf{x}_k & \text{Polyak} \\ \delta_k \mathbf{x}_k + (1 - \delta_k) \mathbf{s}_{k-1} & \text{Nesterov} \end{cases} \quad \triangleright \text{Intermediary point (28a)}$$

$$3: \mathbf{d}_k = \delta_k \mathbf{d}_{k-1} + (1 - \delta_k) \nabla f(\mathbf{y}_k) \quad \triangleright \text{Support dir. (28b)}$$

$$4: \mathbf{s}_k \in S_{\mathcal{D}}(\mathbf{d}_k) \quad \triangleright \text{Support (8)}$$

$$5: \text{if } g(\mathbf{x}_k) \leq \epsilon \text{ then} \quad \triangleright \text{Fixed-point condition (32)}$$

$$6: \quad \text{If } \mathbf{d}_k = \mathbf{x}_k, \text{ return } f(\mathbf{x}_k) \quad \triangleright \text{Algorithm terminates}$$

$$7: \quad \mathbf{s}_k \in S_{\mathcal{D}}(\nabla f(\mathbf{x}_k)) \quad \triangleright \text{Compute } \mathbf{s}_k \text{ in dir. } \nabla f(\mathbf{x}_k)$$

Replace line 3 by:  $\mathbf{d}_k = \mathbf{x}_k$  until termination.

$$8: \widetilde{W}_{k+1} = W_k \cup \{\mathbf{s}_k\} \quad \triangleright \text{Augment active-set}$$

$$9: \mathbf{x}_{k+1} = \text{proj}_{\text{conv}(\widetilde{W}_{k+1})}(\mathbf{0}_{\mathcal{C}}) \quad \triangleright \text{Project } \mathbf{0}_{\mathcal{C}} \text{ on conv}(\widetilde{W}_{k+1})$$

$$10: \text{If } \mathbf{x}_{k+1} = \mathbf{0}_{\mathcal{C}}, \text{ return } 0$$

$$11: W_{k+1} = \{\mathbf{s}^1, \dots, \mathbf{s}^r\} \text{ where } \mathbf{s}^1, \dots, \mathbf{s}^r \text{ are the smallest number of vectors in } \widetilde{W}_{k+1} \text{ such that } \mathbf{x}_{k+1} \text{ is a convex combination of } \mathbf{s}^1, \dots, \mathbf{s}^r.$$

**Stopping criterion.** As the number of iteration  $k$  increases,  $\delta_k \rightarrow 1$  in (28). Therefore,  $\mathbf{d}_k$  tends to be equal to  $\mathbf{d}_{k-1}$  (28b) and thus  $\mathbf{s}_k = \mathbf{s}_{k-1}$  (28c). As a consequence, augmenting  $W_k$  with  $\mathbf{s}_k$  to construct  $\widetilde{W}_{k+1}$  (see (28d)) and then projecting  $\mathbf{0}_{\mathcal{C}}$  onto  $\widetilde{W}_{k+1}$  (28e) will not result in any progress. Therefore,  $\mathbf{x}_{k+1} = \mathbf{x}_k$ : the algorithm reaches a fixed point and is stuck on constant support direction  $\mathbf{d}$ .

In order to cope with this issue, we use the following strategy. Suppose  $\mathbf{x}_k \neq \mathbf{0}_{\mathcal{C}}$ . Since  $\mathbf{x}_k = \text{proj}_{\text{conv}(W_k)}(\mathbf{0}_{\mathcal{C}})$  we have:

$$\forall \mathbf{s}^i \in W_k, \langle \mathbf{x}_k, \mathbf{x}_k - \mathbf{s}^i \rangle = 0. \quad (29)$$

After computing  $\mathbf{s}_k \in S_{\mathcal{D}}(\mathbf{d}_k)$ , if we have:

$$\langle \mathbf{x}_k, \mathbf{x}_k - \mathbf{s}_k \rangle \neq 0, \quad (30)$$

then  $\mathbf{s}_k$  is not a linear combination of vectors in  $W_k$ . Therefore, augmenting  $W_k$  with  $\mathbf{s}_k$  to obtain  $\widetilde{W}_{k+1}$  and projecting  $\mathbf{0}_{\mathcal{C}}$  onto  $\text{conv}(\widetilde{W}_{k+1})$  to obtain  $\mathbf{x}_{k+1}$  will result in the algorithm progressing toward the optimum  $\mathbf{x}^*$ . Suppose on the contrary that:

$$\langle \mathbf{x}_k, \mathbf{x}_k - \mathbf{s}_k \rangle = 0, \quad (31)$$

then  $\mathbf{s}_k$  is a linear combination of vectors in  $W_k$ . Adding  $\mathbf{s}_k$  to  $W_k$  will thus not result in any progress towards the optimum. As a consequence, Eq. (31) encompasses two cases:

- If the support direction  $\mathbf{d}_k$  is aligned with  $\nabla f(\mathbf{x}_k)$ , Eq. (31), corresponding to  $g_{\text{FW}}(\mathbf{x}_k) = 0$ , matches the termination criterion of the distance computation problem and therefore we have reached the optimum i.e  $\mathbf{x}_k = \mathbf{x}^*$ .
- Otherwise, if  $\mathbf{d}_k$  is not aligned with  $\nabla f(\mathbf{x}_k)$ , the algorithm cannot stop as a null duality gap is not met. The algorithm thus enters a cycle where it iterates until Eq. (31) does not hold. To cope with this undesired behavior we simply stop the Polyak or the Nesterov acceleration as soon as Eq. (31) is met and switch back to the non-accelerated version Alg. 4.

1 We thus define the function  $g$  such that for any  $s_k \in \mathcal{D}$ :

$$g(\mathbf{x}_k) = 2\langle \mathbf{x}_k, \mathbf{x}_k - s_k \rangle, \quad (32)$$

2  $g$  is used in Alg. 6 as an optimality criterion ( $g \leq \epsilon$ )  
 3 either for stopping the Polyak and Nesterov accelerations in  
 4 order to continue with the vanilla GJK, or as stopping criteria  
 5 qualifying an optimal solution, in which case  $g = g_{\text{FW}}$  and (18)  
 6 holds. The entire algorithm is summarized in Alg. 6.

7 **Nesterov acceleration for non-strictly convex shapes.** Let us  
 8 explain the effect of the Nesterov acceleration on the support  
 9 direction update (28b) and distinguish between strictly convex  
 10 and non-strictly convex  $\mathcal{D}$ :

- 11 • If  $\mathcal{D}$  is strictly convex, any vector  $s$  belonging to the  
 12 surface of  $\mathcal{D}$  has a unique corresponding direction  $\mathbf{d}$  such  
 13 that  $s = S_{\mathcal{D}}(\mathbf{d})$ . Here, we stress the fact that the support  
 14 function  $S_{\mathcal{D}}$  returns only *one* vector. Consequently, we  
 15 have  $\mathbf{d}_k \neq \mathbf{d}_{k-1}$  and therefore  $s_k \neq s_{k-1}$ . The fixed  
 16 point condition (31) is thus not met unless  $\delta_k = 1$   
 17 and Nesterov acceleration continues to be applied in  
 18 Alg. 6. In practice, the algorithm runs until  $\delta_k$  gets close  
 19 to 1 or  $\mathbf{x}_k$  gets close to  $\mathbf{0}_c$ . The condition (31) is then  
 20 satisfied as the algorithm starts to cycle. The Nesterov  
 21 acceleration is thus removed and the algorithm runs until  
 22 the convergence criteria is satisfied, guaranteed by the  
 23 Frank-Wolfe algorithm.
- 24 • Otherwise, if  $\mathcal{D}$  is non-strictly convex, multiple support  
 25 directions  $\{\mathbf{d}^1, \dots, \mathbf{d}^m, \dots\}$  can yield the same support  
 26 vector  $s \in S_{\mathcal{D}}(\mathbf{d}^1) = \dots = S_{\mathcal{D}}(\mathbf{d}^m) = \dots$  etc. Conse-  
 27 quently, it is possible to have  $\mathbf{d}_{k-1} \neq \mathbf{d}_k$  and  $s_k = s_{k-1}$ .  
 28 Therefore, even though  $\delta_k$  is not close to 1, the fixed point  
 29 condition (31) can be verified. The Nesterov acceleration  
 30 is stopped, possibly prematurely.

31 The latter case is especially problematic when shapes  $\mathcal{A}_1$   
 32 and  $\mathcal{A}_2$  are in close-proximity, which is ultimately the type  
 33 of collision problems commonly encountered in simulation or  
 34 motion planning with contacts. In (28b), this is due to the  
 35 norm of  $\nabla f(\mathbf{y}_k)$  being predominant over the norm of  $\mathbf{d}_{k-1}$   
 36 as  $k$  increases,  $\|\mathbf{d}_{k-1}\| \ll \|\nabla f(\mathbf{y}_k)\|$ . As a consequence, the  
 37 Nesterov acceleration enters a cycle: the support direction  $\mathbf{d}_k$   
 38 does not change enough compared to  $\mathbf{d}_{k-1}$ , hence the support  
 39 point  $s_k$  is identical to  $s_{k-1}$  and therefore the intermediary  
 40 point  $\mathbf{y}_k$  does not change and the cycle repeats. As a conse-  
 41 quence, the criterion (31) is met and the Nesterov acceleration  
 42 is stopped to escape the cycle, possibly prematurely. To  
 43 prevent this phenomenon observed on non-strictly convex  $\mathcal{D}$ ,  
 44 we propose to replace (28b) by a simple heuristic which  
 45 normalizes the gradient and momentum directions as follows:

$$\mathbf{d}_k = \delta_k \frac{\mathbf{d}_{k-1}}{\|\mathbf{d}_{k-1}\|} + (1 - \delta_k) \frac{\nabla f(\mathbf{y}_k)}{\|\nabla f(\mathbf{y}_k)\|}, \quad (33)$$

46 summarized in Alg. 7. In Sec. IV, we experimentally prove  
 47 this heuristic to significantly reduce the number of steps for  
 48 distance computations for non-strictly convex shapes. We also  
 49 show that this heuristic does not need to be applied to the  
 50 Polyak acceleration, as, contrary to the Nesterov acceleration,  
 51 the Polyak acceleration does not compute an intermediary  
 52 point  $\mathbf{y}_k$ .

---

**Algorithm 7** Normalize direction for non-strictly convex shapes in Nesterov-accelerated GJK

---

Replace line 3 in Alg. 6 by:

$$1: \mathbf{d}_k = \delta_k \frac{\mathbf{d}_{k-1}}{\|\mathbf{d}_{k-1}\|} + (1 - \delta_k) \frac{\nabla f(\mathbf{y}_k)}{\|\nabla f(\mathbf{y}_k)\|}$$


---

## IV. EXPERIMENTS

In this section, we study the performance of both Polyak and Nesterov-accelerated GJK (Alg. 6) against the vanilla GJK (Alg. 4) algorithm.

In sections IV-A and IV-B, we benchmark our proposed Polyak-accelerated and Nesterov-accelerated GJK algorithms against the vanilla GJK algorithm on these two distinct benchmarks. The benchmark made of strictly-convex shapes represents a worst-case scenario regarding the number of iterations for all variants of GJK. The benchmark of non-strictly convex shapes represents shapes typically used in robotic or computer graphics applications. In Sec. IV-C, we benchmark GJK and our proposed accelerated gradients against the state-of-the-art quadratic programming solver ProxQP [50]. We show that GJK and our proposed accelerated variants vastly outperform generic quadratic programming (QP) solvers, making these QP solvers prohibitive for collision detection. Then, in Sec. IV-D, we compare our methods and our implementation of vanilla GJK against different collision detection solvers of various collision detection libraries. Finally, in Sec. IV-E, we benchmark vanilla, Polyak-accelerated, and Nesterov-accelerated GJK on a dataset of trajectories obtained using a physics simulator. We show that, similarly to vanilla GJK, our accelerated GJK algorithms can benefit from being warm-started with previous simulation time steps, outperforming the vanilla GJK in physics simulation scenarios.

**Implementation.** We leverage the HPP-FCL C++ library [28], [51], an extension of the original FCL library [28]. Unlike FCL, HPP-FCL provides its own implementation of GJK, which we have extended by implementing the Polyak and Nesterov-accelerated GJK algorithms (Alg. 6). The open-source code of the HPP-FCL library is publicly available at <https://github.com/humanoid-path-planner/hpp-fcl> under the BSD-3 license. The benchmark code is publicly available at <https://github.com/lmontaut/colbench> under the GNU AGP License.

**Shapes datasets.** To distinguish between pairs of strictly convex and non-strictly convex shapes, we build a first benchmark only composed of pairs of ellipsoids (strictly convex shapes) and a second benchmark using pairs of standard meshes (represented by their convex hulls) which are taken from the commonly-used YCB dataset [52].

**Ellipsoids.** In the ellipsoids benchmark, the ellipsoids are randomly generated by sampling positive-definite matrices. In total, we generate 1000 random pairs of ellipsoids. Given a pair of ellipsoids, we randomly sample relative poses between the shapes, using a uniform distribution for the relative rotation between the shapes. Regarding the translation part of the random poses, the directions are selected at random, but the norms are chosen so that we control the distance  $\text{dist}(\mathcal{A}_1, \mathcal{A}_2)$

1 between the objects. This enables us to measure the influ-  
 2 ence of the separation distance on the performance of the  
 3 studied algorithms. The values used for  $\text{dist}(\mathcal{A}_1, \mathcal{A}_2)$  range  
 4 from  $-0.1$  m to  $1$  m. Negative values correspond to scenarios  
 5 where the shapes intersect, with  $\text{dist}(\mathcal{A}_1, \mathcal{A}_2)$  correspond-  
 6 ing to the separating vector’s norm. The separating vector is the  
 7 vector of the smallest norm needed to translate one of the two  
 8 shapes such that the two shapes do not intersect. Therefore, for  
 9 each pair of ellipsoids, 100 random relative poses are sampled,  
 10 so the shapes do not intersect. We translate the shapes along  
 11 the axis given by their closest points for each relative pose to  
 12 study the impact of  $\text{dist}(\mathcal{A}_1, \mathcal{A}_2)$ . We then set  $\text{dist}(\mathcal{A}_1, \mathcal{A}_2)$  to  
 13 fixed values between  $-0.1$  m to  $1$  m.

14 **YCB meshes.** On the other hand, the YCB mesh dataset  
 15 contains about 60 shapes commonly used for robotic ma-  
 16 nipulation tasks (kitchen appliances, tools, toys, etc.). Each  
 17 object has three different resolution levels corresponding to  
 18 the number of points representing the mesh. For each object,  
 19 we take the lowest resolution, i.e., the *google-16k* versions of  
 20 the meshes, as it is resolute enough for any robotic task. As  
 21 GJK-like algorithms work on convex shapes, we pre-compute  
 22 the convex hulls of each object in the YCB dataset. This  
 23 procedure needs only to be done once; if more precision is  
 24 required for a certain robotic task, it is common to decompose  
 25 a non-convex object into a set of convex sub-objects. For  
 26 the sake of simplicity, we will not decompose YCB objects  
 27 into sub-objects, as the results presented in this section would  
 28 essentially be the same. In the rest of this section, when we  
 29 mention a shape, we refer to its convex hull unless explicitly  
 30 stated otherwise. The resulting meshes extracted from the YCB  
 31 dataset contain between 100 and 8000 vertices. About 50%  
 32 of meshes contain between 100 and 1000 vertices. As in the  
 33 ellipsoids benchmark, 100 random relative poses are sampled  
 34 for each pair such that the shapes do not intersect and then  
 35 set  $\text{dist}(\mathcal{A}_1, \mathcal{A}_2)$  to fixed values between  $-0.1$  m and  $1$  m.

36 In both benchmarks (ellipsoids and YCB meshes), the  
 37 characteristic sizes of the shapes range from a few centimeters  
 38 up to a meter. Finally, for the distance computation problem,  
 39 we select a convergence tolerance of  $\epsilon = 10^{-8}$ .

40 **Initialization strategy.** Apart from Sec. IV-E, the GJK al-  
 41 gorithm and our proposed accelerated GJK algorithms are  
 42 initialized with the centers of the shapes’ bounding boxes. The  
 43 bounding box of a shape fully encapsulates it, as is shown in  
 44 Fig. 1. Hence, if we denote  $c_1$  and  $c_2$  the geometric centers of  
 45 the bounding boxes of  $\mathcal{A}_1$  and  $\mathcal{A}_2$ , then we initialize vanilla  
 46 GJK, Polyak-accelerated GJK and Nesterov-accelerated GJK  
 47 to  $x_0 = c_1 - c_2$ .

48 **Metrics.** To measure the performances of Polyak-accelerated  
 49 GJK, Nesterov-accelerated GJK, and the vanilla GJK algo-  
 50 rithms, we measure the number of iterations  $N^k$  to solve a  
 51 given collision problem. For the mesh benchmark, we also  
 52 measure the execution time  $T^\mu$  of both methods. We solve  
 53 each generated collision problem 100 times to cope with CPU  
 54 throttling. We then report the average of the 90% lowest  
 55 computation times. All the benchmarks in this paper were run  
 56 on an Apple M1 Max CPU.

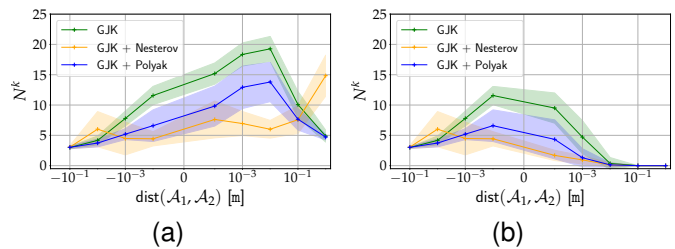


Fig. 7. Comparison of Polyak-accelerated GJK, Nesterov-accelerated GJK, and vanilla GJK on the ellipsoid benchmark for (a) distance computation and (b) Boolean collision checking. The graphs show the number of iterations (y-axis) vs. the signed distance between the two shapes (x-axis). The curve shows the mean value over 100,000 random trials. The shaded region corresponds to the standard deviation. The Nesterov-accelerated GJK algorithm requires fewer iterations when the shapes are in close proximity. The Polyak-accelerated GJK algorithm is more robust when shapes are strongly overlapping or distant.

#### A. Worst case scenario: strictly convex shapes - ellipsoids

1 We first focus on the ellipsoid benchmark to get a statistical  
 2 understanding of the performance of Polyak and Nesterov-  
 3 accelerated GJK against vanilla GJK. In the following, we  
 4 explain why these shapes are interesting to study experimen-  
 5 tally, as they represent the worst-case scenario that GJK-  
 6 like algorithms can be confronted with. First, as previously  
 7 explained, GJK-like algorithms look for the optimal active set  
 8 of the solution  $x^*$ . Otherwise said, GJK-like methods find  
 9 a set of support points  $W^* = \{s^1, s^2, \dots\}$  such that the  
 10 optimal solution  $x^*$  is a convex combination of the points  
 11 of  $W^*$ , where  $s^i$  are support points computed while running  
 12 GJK or our proposed accelerations. Then, contrary to non  
 13 strictly-convex shapes, strictly-convex shapes have an infinite  
 14 amount of support points. As explained at the end of Sec. III,  
 15 each normalized support direction  $d$  corresponds to a unique  
 16 support point  $S_D(d)$ . Therefore, it is fundamentally harder  
 17 to identify the optimal active set when considering strictly-  
 18 convex shapes, as there is an infinite amount of potential  
 19 support points to consider. In contrast, there is a finite amount  
 20 of support points to consider when using non strictly-convex  
 21 shapes.  
 22

23 In Fig. 7, we show the performance of the vanilla, the  
 24 Polyak-accelerated, and the Nesterov-accelerated GJK algo-  
 25 rithms on the ellipsoids benchmark. Fig. 7a and Fig. 7b  
 26 show the mean and standard deviation of the number of  
 27 iterations  $N^k$  of each method for the distance computation  
 28 and the Boolean collision checking problems, respectively. When  
 29 the shapes are shallowly intersecting, Polyak and Nesterov-  
 30 accelerated GJK converge with the same or even fewer number  
 31 of iterations than vanilla GJK. However, the shallower the  
 32 penetration, the more Polyak and Nesterov accelerate over  
 33 vanilla GJK, with Nesterov providing the most acceleration.  
 34 The irregularity in standard deviation at  $-0.01$  m is a crit-  
 35 ical zone for the Nesterov momentum where the variance  
 36 increases. When shapes are in close proximity, the Nesterov  
 37 acceleration of GJK significantly reduces the number of  
 38 iterations compared to vanilla GJK and Polyak-accelerated  
 39 GJK. Finally, when shapes are distant,  $1 \text{ m} \leq \text{dist}(\mathcal{A}_1, \mathcal{A}_2)$ ,  
 40 the Nesterov acceleration is detrimental to convergence on  
 41 the distance computation problem while Polyak-accelerated

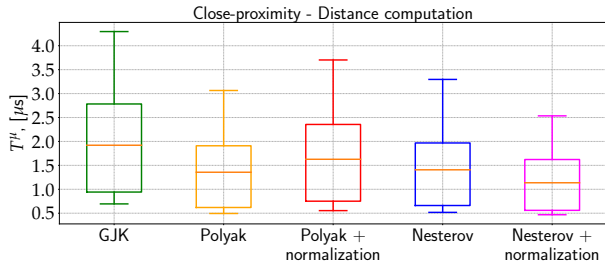


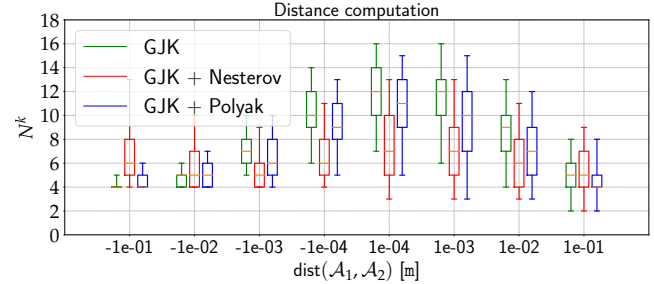
Fig. 8. Impact of support direction normalization in Polyak and Nesterov-accelerated GJK on the YCB benchmark. The graph shows the computation time  $T^\mu$  (lower is better) for vanilla GJK, Polyak-accelerated GJK, and Nesterov-accelerated GJK with and without support direction normalization. Here, the two shapes are in close-proximity:  $0 \text{ m} < \text{dist}(\mathcal{A}_1, \mathcal{A}_2) \leq 0.1 \text{ m}$ . Normalizing the support direction benefits Nesterov-accelerated GJK, reducing the overall number of iterations compared to GJK and non-normalized Nesterov-accelerated GJK.

1 GJK remains competitive against vanilla GJK. This indicates  
 2 that the Polyak acceleration is generally more robust than  
 3 the Nesterov acceleration. However, it offers less acceleration  
 4 over vanilla GJK when the shapes are in close-proximity  
 5 or shallowly overlapping. A similar pattern of speed-ups of  
 6 Polyak and Nesterov-accelerated GJK over vanilla GJK is  
 7 shown for the collision detection problem in Fig. 7b.

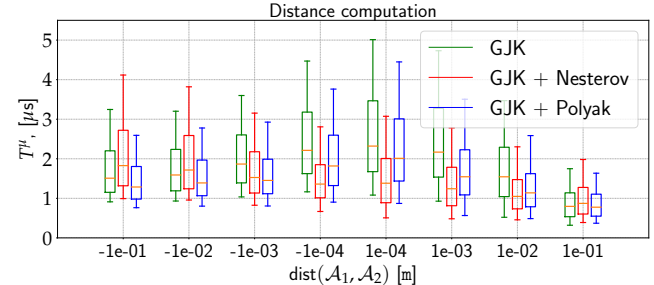
#### 8 B. Non-strictly convex shapes: meshes

9 **Effect of support direction normalization.** For meshes, the  
 10 importance of normalizing the support direction (see Eq. (33))  
 11 in the Nesterov-accelerated GJK is highlighted in Fig. 8. For  
 12 both the distance computation and Boolean collision checking  
 13 problems, the normalization heuristic prevents the Nesterov  
 14 acceleration from reaching a fixed point too early, and con-  
 15 sequently, it reduces the overall amount of iterations needed  
 16 to converge. This is, however, not the case for the Polyak-  
 17 accelerated GJK algorithm, which does not benefit from sup-  
 18 port normalization. As explained at the end of Sec. III, the  
 19 Polyak acceleration does not compute an intermediary point,  
 20 unlike the Nesterov acceleration scheme. In the following, we  
 21 thus focus only on Polyak-accelerated GJK *without* support  
 22 normalization and Nesterov-accelerated GJK *with* support  
 23 normalization. We compare the performances of these two  
 24 algorithms against the vanilla GJK algorithm.

25 **Statistical validation over the YCB dataset.** In Fig. 9 and  
 26 Fig. 10, we report the number of iterations  $N^k$  and execution  
 27 time  $T^\mu$  for Polyak-accelerated GJK, Nesterov-accelerated  
 28 GJK and vanilla GJK. In Fig. 11, we report relative accel-  
 29 erations  $T_{\text{GJK}}^\mu / T_{\text{polyak}}^\mu$  and  $T_{\text{GJK}}^\mu / T_{\text{Nesterov}}^\mu$   
 30 of Polyak-accelerated compared to GJK. These relative accel-  
 31 erations are computed on a given collision problem, and Fig. 11  
 32 reports their statistical distributions. These relative measures  
 33 allow analyzing the effects of the studied algorithms on the  
 34 same collision problems, which are not captured when using  
 35 absolute values. Overall, Polyak and Nesterov-accelerated  
 36 GJK significantly reduce the execution time when compared  
 37 to GJK in cases where shapes are shallowly intersecting or  
 38 in close-proximity. It is worth recalling, at this stage,  
 39 that when two shapes are relatively far from each other, any  
 broadphase algorithm will

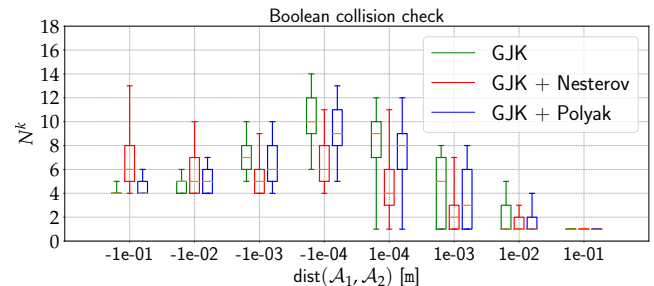


(a)

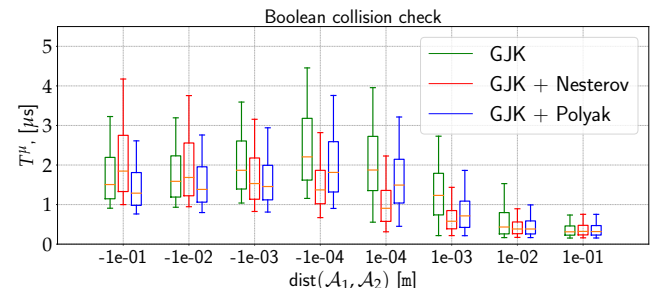


(b)

Fig. 9. Distance computation on the YCB benchmark. The graphs show the number of iterations  $N^k$  (a) and the execution time  $T^\mu$  (b) for Polyak-accelerated GJK, Nesterov-accelerated GJK (with normalization) and vanilla GJK for a range of distances (x-axis) between the shapes. For both metrics, lower is better.



(a)






(b)

Fig. 10. Boolean collision check on the YCB benchmark. The graphs show the number of iterations  $N^k$  (a) and the execution time  $T^\mu$  (b) for the Polyak-accelerated GJK, Nesterov-accelerated GJK (with normalization), and vanilla GJK algorithms for a range of distances (x-axis) between the shapes. For both metrics, lower is better.



TABLE I  
COMPUTATION TIMES ( $\mu s$ ) FOR DISTANCE COMPUTATION ( $T_D^\mu$ ) AND BOOLEAN COLLISION CHECKING ( $T_C^\mu$ ) ON THE YCB BENCHMARK FOR CLOSE-PROXIMITY OR SHALLOWLY INTERSECTING SHAPES.  $N$  DENOTES THE NUMBER OF VERTICES FOR EACH MESH.

		$N = 240$			$N = 1811$			$N = 3585$		
		GJK	Polyak	Nesterov	GJK	Polyak	Nesterov	GJK	Polyak	Nesterov
	$T_D^\mu$	$1.1 \pm 0.3$	<b><math>0.9 \pm 0.3</math></b>	<b><math>0.9 \pm 0.3</math></b>	$1.9 \pm 0.5$	$1.5 \pm 0.5$	<b><math>1.4 \pm 0.5</math></b>	$3.2 \pm 0.8$	<b><math>2.3 \pm 0.7</math></b>	$2.4 \pm 0.7$
	$T_C^\mu$	$0.9 \pm 0.4$	<b><math>0.7 \pm 0.4</math></b>	$0.8 \pm 0.4$	$1.5 \pm 0.6$	$1.2 \pm 0.6$	<b><math>1.1 \pm 0.6</math></b>	$2.5 \pm 0.9$	<b><math>1.7 \pm 0.8</math></b>	$1.9 \pm 1.0$
	$T_D^\mu$				$2.7 \pm 0.8$	$2.1 \pm 0.7$	<b><math>1.9 \pm 0.6</math></b>	$4.0 \pm 1.0$	<b><math>2.9 \pm 0.9</math></b>	$2.9 \pm 1.0$
	$T_C^\mu$				$2.3 \pm 0.8$	$1.6 \pm 0.8$	<b><math>1.5 \pm 0.8</math></b>	$3.1 \pm 1.2$	<b><math>2.1 \pm 1.0</math></b>	$2.2 \pm 1.3$
	$T_D^\mu$							$4.4 \pm 1.3$	<b><math>2.9 \pm 1.0</math></b>	$3.0 \pm 0.9$
	$T_C^\mu$							$3.0 \pm 1.9$	<b><math>2.1 \pm 1.4</math></b>	<b><math>2.1 \pm 1.4</math></b>

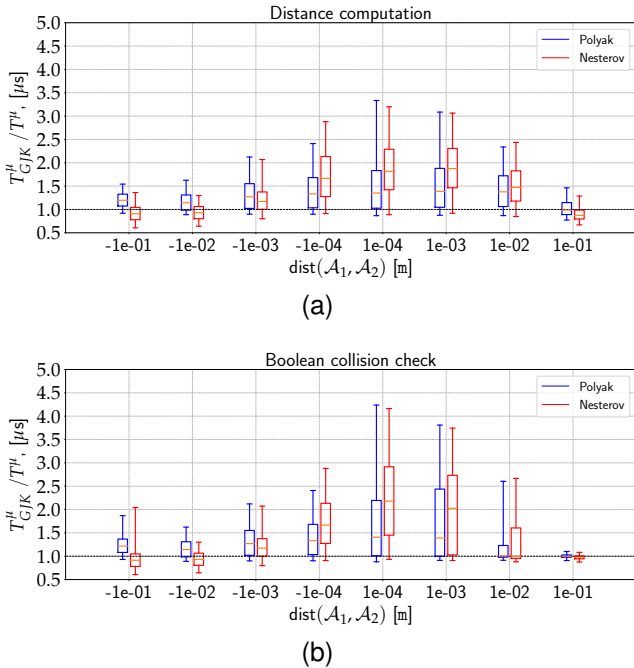


Fig. 11. Speed-ups of Polyak and Nesterov-accelerated GJK over vanilla GJK on the YCB benchmark. The plots show ratios of the number of execution times for (a) distance computation and (b) boolean collision checking of Polyak-accelerated GJK and Nesterov-accelerated GJK (with normalization) against vanilla GJK. Ratios over 1.0 show speed-ups of accelerated GJK over vanilla GJK. For both metrics, higher is better.

more robust than Nesterov-accelerated GJK as it is almost always better than vanilla GJK, even when the shapes are distant or overlap.

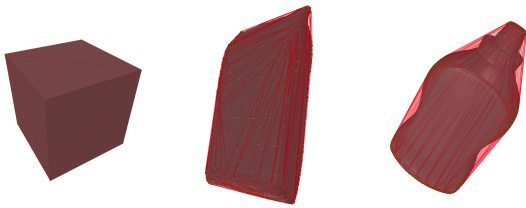
In Table. I, we select three meshes with an increasing number of vertices to highlight the benefits of the Polyak and Nesterov accelerations. For each pair, we report the mean and the standard deviation of the execution time for distance computation and Boolean collision checking. We consider the challenging set-up of close-by or shallowly intersecting shapes in the range of separation distances  $-0.01 \text{ m} \leq \text{dist}(\mathcal{A}_1, \mathcal{A}_2) \leq 0.01 \text{ m}$ . The lower mean and standard deviation show that Polyak and Nesterov-accelerated GJK are faster than the vanilla GJK and reduce the spread of computation times across the different collision problems in this setting.

From this benchmark involving shapes from the YCB dataset, we can distinguish two use cases in which one would prefer using Polyak-accelerated GJK compared to Nesterov-accelerated and vice-versa. In tasks where the exact distance between the shapes needs to be computed and where this distance separating the shapes can take any value, due to its robustness, the Polyak-accelerated GJK algorithm is better suited than its Nesterov counterpart. However, in a situation involving shapes interacting at close proximity, like in a contact physics simulation, it is preferable to choose the Nesterov-accelerated GJK. Before studying the performance of GJK and our proposed accelerations for physics simulation, we first show the benefits of using GJK-based algorithms for collision detection instead of standard off-the-shelf optimization solvers and provide a comparison of the implementations of our methods against baselines from other collision detection libraries.

1 automatically discard such a pair. Only in a small percentage  
 2 of cases, Polyak-accelerated GJK and Nesterov-accelerated  
 3 GJK are slower than GJK. When measuring the absolute  
 4 performance of the two proposed methods, Polyak-accelerated  
 5 GJK provides less acceleration than Nesterov-accelerated GJK  
 6 in critical cases with close proximity and shallowly overlap-  
 7 ping collision problems. However, Polyak-accelerated GJK is

1  
2  
3  
4  
5  
6  
7  
8  
9  
10  
11  
12  
13  
14  
15  
16  
17  
18  
19  
20  
21  
22  
23  
24  
25  
26  
27  
28  
29  
30  
31  
32

TABLE II  
COMPUTATION TIME IN MICRO-SECONDS OF GJK-LIKE SOLVERS VS.  
SOTA QUADRATIC PROGRAMMING PROXQP SOLVER.



	$N_v = 8$ $N_f = 6$	$N_v = 250$ $N_f = 496$	$N_v = 940$ $N_f = 1876$
ProxQP	$5.3 \pm 2.7 \mu s$	$(2 \pm 0.6) \cdot 10^3 \mu s$	$(20 \pm 14) \cdot 10^3 \mu s$
GJK	$0.2 \pm 0.03 \mu s$	$0.8 \pm 0.3 \mu s$	$2.1 \pm 0.5 \mu s$
Nesterov	$0.2 \pm 0.05 \mu s$	$0.7 \pm 0.2 \mu s$	$1.4 \pm 0.3 \mu s$
Polyak	$0.2 \pm 0.05 \mu s$	$0.6 \pm 0.2 \mu s$	$1.4 \pm 0.4 \mu s$

difference. Therefore, since GJK and EPA are made to work in succession with one another, it is almost always the case that physics simulators use GJK to first detect collisions and then EPA to compute contact features if a collision is detected. All the libraries listed before are written either in C or in C++.

In Fig. 12, we report the performance of the methods listed before on the YCB benchmark used in Sec. IV-B. We measure the execution time of the different collision detection solvers on the boolean collision check task and divide the results into three distance categories: when shapes are distant ( $\text{dist}(\mathcal{A}_1, \mathcal{A}_2) \geq 1\text{m}$ ), when shapes are in close-proximity ( $0\text{m} \leq \text{dist}(\mathcal{A}_1, \mathcal{A}_2) \leq 0.1\text{m}$ ) and when shapes are overlapping ( $\text{dist}(\mathcal{A}_1, \mathcal{A}_2) \leq 0\text{m}$ ). The collision problems corresponding to the *distant* case would typically be filtered by the broadphase. We report them to give a clear picture of the performance of the different implementations. In practice, the *close-proximity* and *overlapping* cases correspond to situations when the different collision detection solvers are actually called; the broad phase cannot filter such collision problems and the narrow phase is then called.

The results show our implementation of GJK and our proposed methods outperform the solvers of the other collision detection libraries. We find similar results for the distance computation task. We now turn our attention to the context of physics simulation and show that our proposed methods, just like GJK, can be warm-started by using previous simulation steps.

### E. Collision detection for physics simulation

In the previous benchmarks, we have experimentally shown the improvement of our methods, Polyak-accelerated GJK and Nesterov-accelerated GJK, over the vanilla GJK algorithm for collision problems which are important in practice, *i.e.* when the broadphase has not filtered collision pairs and are thus overlapping or in close proximity. So far, the benchmarks have been constructed by randomly selecting poses for our shapes. However, in robotics applications such as trajectory optimization, motion planning, or computer graphics, the successive poses between objects are usually correlated by time. In this sub-section, we study how vanilla GJK, Polyak-accelerated GJK, and Nesterov-accelerated GJK can be warm-started using the previous time instant, as occurring inside physics simulators.

To do so, we create a dataset of trajectories using pairs of objects from the YCB dataset used in Sec. IV-B. We randomly select 1000 pairs of YCB objects and drop them in a funnel as shown in Fig. 14. At the beginning of the simulation, each object is given a random pose and random translational and rotational velocities. The simulation is then run at 120Hz for 1 second. When a collision occurs, the GJK and EPA (expanding polytope algorithm) algorithms are called to determine the position of the contact points and the corresponding normal for the considered pair of objects. The collision is then resolved using a contact solver based on the Projected Gauss-Seidel [57] algorithm to account for a second-order cone representing friction, following the implementation proposed in [58]. In total, 120k collision problems are generated. For

### C. GJK-like algorithms vs. generic quadratic programming solvers

As explained in Sec. II, in the case of two convex meshes, the collision problem can be formulated as a Quadratic Program (2) (QP), which can be solved using any generic QP solver [50], [53]–[56]. In Table II, we compare the performance of GJK and our proposed accelerations against the state-of-the-art ProxQP solver [50]. We report the computation timings in micro-seconds for pairs of identical shapes with an increasing number of vertices ( $N_v$ ) and faces ( $N_f$ ). The results are staggering: for very simple convex meshes like a cube, GJK, and its accelerated variants are already more than 10 times faster than the QP solver. When the complexity of the meshes increases, GJK and its variants are thousands to tens of thousands of times faster than the QP solver, making generic QP solvers prohibitive for collision detection in real-time applications like robotics or computer graphics. Although these results are not surprising, they clearly showcase why dedicated solvers such as GJK-like methods are crucial for collision detection.

### D. Comparison against other collision detection libraries

In this sub-section, we compare our implementations of vanilla, Nesterov-accelerated and Polyak-accelerated GJK against the following baselines from other collision detection libraries: CCD’s MPR and GJK implementations [15], FCL’s GJK implementation [16] and Bullet’s GJK implementation. These collision detection algorithms are used in physics simulators like Drake [18], MuJoCo [3], ODE [19] and Bullet [1]. Since GJK is the state-of-the-art algorithm for narrow phase collision detection, it is no surprise that most collision detection libraries implement only this algorithm. In addition to being a general, robust and computationally fast method, GJK-like algorithms also have the advantage of producing a simplex surrounding the origin when shapes are in collision (see Sec. II). This simplex is then fed to the Expanding Polytope Algorithm (EPA) in order to estimate the penetration depth and separation vector [22]; these contact informations are used in physics simulation to resolve contact constraints. Just like GJK, the core of EPA consist in computing support points in order to expand a polytope inside the Minkowski

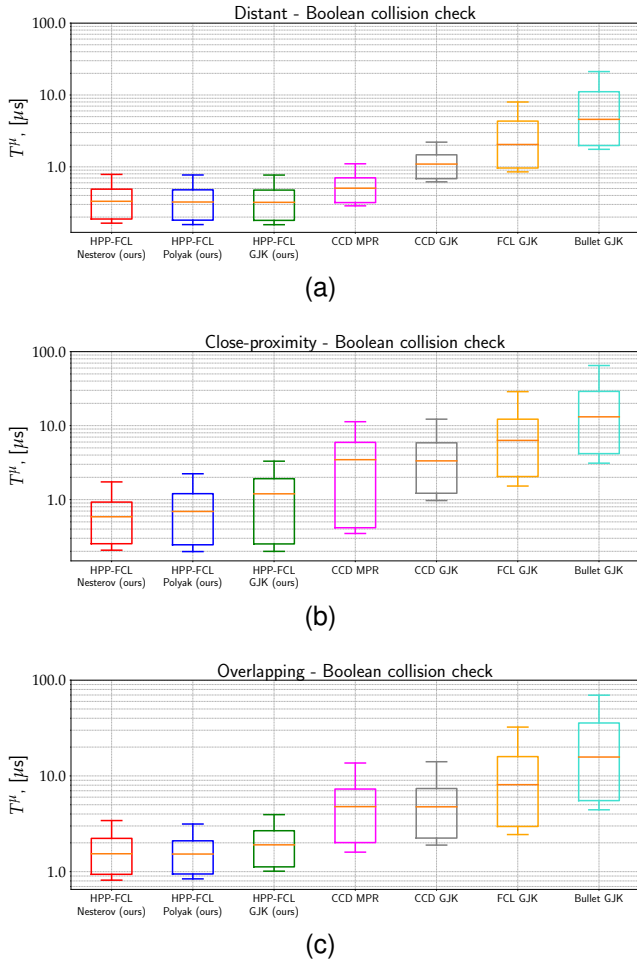


Fig. 12. Computation time in micro-seconds of implementations of different collision detection solvers from various C/C++ libraries on the YCB benchmark for boolean collision checking. The y-axis is a log-scale. We compare our implementation of vanilla GJK, Nesterov-accelerated GJK and Polyak-accelerated GJK against FCL’s GJK implementation, CCD’s GJK implementation and CCD’s MPR implementation. The results are split into three different categories: (a) when shapes are distant ( $\text{dist}(\mathcal{A}_1, \mathcal{A}_2) \geq 1\text{m}$ ), (b) in close-proximity ( $0 \leq \text{dist}(\mathcal{A}_1, \mathcal{A}_2) \leq 0.1\text{m}$ ) and (c) overlapping ( $\text{dist}(\mathcal{A}_1, \mathcal{A}_2) \leq 0\text{m}$ ). Lower is better.

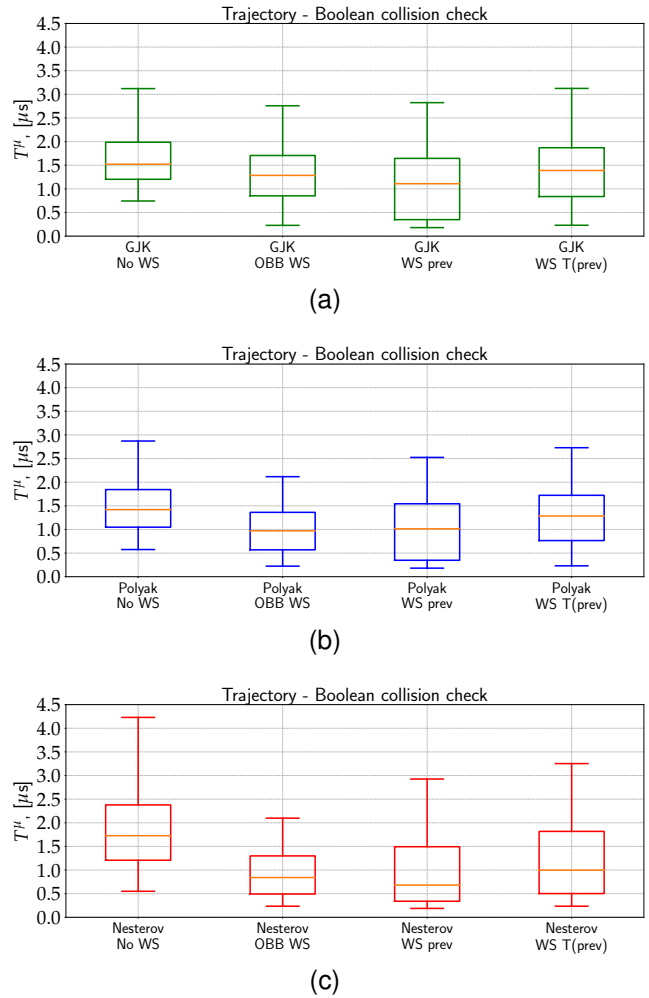


Fig. 13. Boolean collision checking of YCB objects’ trajectories (see Fig. 14) for different warm-start strategies for (a) vanilla GJK, (b) Polyak-accelerated GJK, and (c) Nesterov-accelerated GJK (with normalization). In the three figures, *WS* is an abbreviation of *warm-start*. The *No WS* strategy signifies the algorithm is initialized with  $\mathbf{x}_0 = (1, 0, 0)^T$ . The *OBB WS* strategy uses the objects’ current OBBs centers to compute  $\mathbf{x}_0$ . In both *WS prev* and *WS T(prev)*,  $\mathbf{x}_0$  is computed using GJK or EPA’s previous solution, when this solution is available (i.e., when the previous collision problem was not discarded by the broadphase). Contrary to *WS prev*, *WS T(prev)* corrects the previous solution using the relative displacement of the shapes between the two considered time steps.

1 each collision problem, we extract the YCB shapes and their  
2 poses.

3 This dataset allows us to evaluate the vanilla, Polyak-  
4 accelerated, and Nesterov-accelerated GJK algorithms on the  
5 same collision problems generated by a physics simulation.  
6 Interestingly, this dataset allows us to study only the collision  
7 problems not filtered by the broadphase of the physics simula-  
8 tor, as explained in Sec. I. During the broad phase, the oriented  
9 bounding boxes of the objects (OBBs, as shown in Fig. 1) are  
10 used to assess if objects are not in collision. Therefore, if the  
11 broad phase does not filter a collision, the GJK algorithm and  
12 our proposed accelerations are called and solve the boolean  
13 collision check problem. Finally, this dataset allows us to test  
14 different strategies to warm-start (WS) the GJK algorithm and  
15 our proposed accelerations. We denote by  $\mathbf{x}_0^t$  the initial guess  
16 given to vanilla, Polyak-accelerated and Nesterov-accelerated  
17 GJK at time step  $t$  of the simulation. We also denote by  $\mathbf{x}^{t-1}$   
18 the separation vector found by GJK (accelerated or not) or  
19 EPA at time-step  $t - 1$  of the simulation. We consider four

different warm-start strategies for the vanilla GJK algorithm  
and our proposed accelerations:

- 1) the first strategy is the *No WS* strategy, where the vanilla, Polyak, and Nesterov GJK algorithms are initialized using  $\mathbf{x}_0^t = (1, 0, 0)^T$ . This strategy serves as a baseline for the other warm-start strategies.
- 2) The second strategy is the *OBB WS* strategy, where  $\mathbf{x}_0^t = \mathbf{c}_1^t - \mathbf{c}_2^t$  with  $\mathbf{c}_1^t$  and  $\mathbf{c}_2^t$  being the centers of the considered objects’ oriented bounding boxes. This warm-start is used in all the previous benchmarks, as explained at the beginning of this section.
- 3) The third strategy is the *WS prev* strategy, where  $\mathbf{x}_0 = \mathbf{x}^{t-1}$  is initialized using the solution found by GJK or EPA in the previous simulation time step.
- 4) The fourth and last strategy is the *WS T(prev)* strategy. The difference with the *WS prev* strategy is that we use

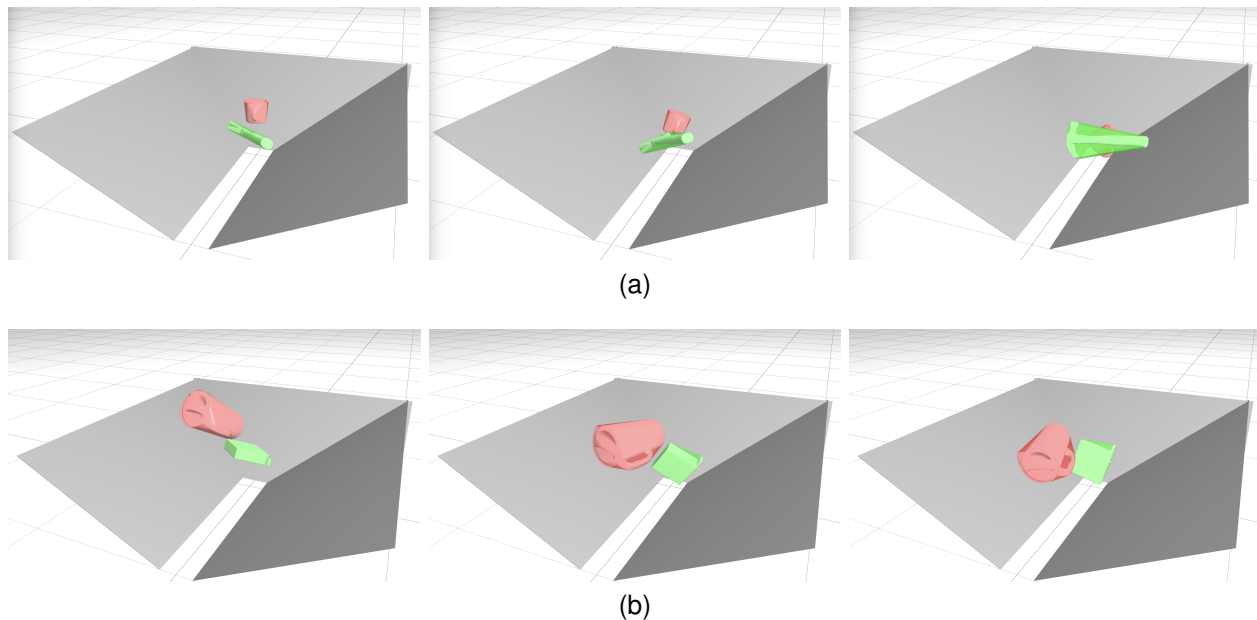


Fig. 14. Two different trajectories (a) and (b) with two different pairs of objects from the YCB dataset. The objects are dropped with a random initial velocity for each trajectory in a funnel (the grey walls). At each time step, if the broadphase cannot discriminate if the shapes are in collision or not, we use the vanilla GJK algorithm or our proposed Polyak and Nesterov-accelerated variants of GJK to determine if a collision occurs between the convex-hulls of the collision pair.

the relative transformation of the shapes between time steps  $t$  and  $t - 1$  to anticipate how  $\mathbf{x}^{t-1}$  might move between these two time steps.

The last two warm-starting strategies might not always be actionable. Indeed, if at time step  $t - 1$  the broad phase finds no collision between the two considered shapes, the GJK and EPA algorithms are not called, and therefore,  $\mathbf{x}^{t-1}$  does not exist. Consequently, if GJK needs to be called at time step  $t$ , it cannot use  $\mathbf{x}^{t-1}$ . In such a case, these two strategies fall back to the second strategy, which exploits the objects' OBBs.

We run vanilla, Polyak-accelerated and Nesterov-accelerated GJK on the dataset of trajectories described previously; the results of this benchmark are summed up in Fig. 13. In this figure, we report the computation time of the boolean collision check for GJK and our proposed accelerations. Importantly, this figure only considers the collision problems which were not filtered by the broad phase, as GJK or its accelerations would not be called otherwise. In doing so, we aim to provide the clearest possible picture of the computation time dedicated to GJK in a physics computation. Due to the filtering of the broad phase, the typical distance separating the shapes is less than a few centimeters; this corresponds to the overlapping and close-proximity cases described in the previous benchmarks. First, the results show that for the three studied methods, the *No WS* and *WS T(prev)* warm-start strategies provided a worse initial guess than the two other warm-start strategies. It appears that the *WS T(prev)* strategy is often the worse strategy; this observation means that the separation vector computed by GJK and/or EPA moves in a non-trivial manner between time steps  $t - 1$  and  $t$  of the simulation. For vanilla GJK, the best warm-starting strategy is the *WS prev* strategy, which re-uses the separation vector computed by GJK and EPA at

time step  $t - 1$  of the simulation. For Polyak-accelerated GJK, both the *OBB WS* and *WS prev* strategies perform better than vanilla GJK's best warm-starting strategy. However, contrary to GJK, the *OBB WS* strategy is arguably better than the *WS prev* strategy as it greatly reduces the variance of the computation timings distribution. For Nesterov-accelerated GJK, the results are even more significant: both the *OBB WS* and *WS prev* strategy significantly outperform GJK with its best warm-starting strategy. When using the *OBB WS* and *WS prev* strategies, the Nesterov acceleration allows the median of computation times to reach close to  $0.5\mu\text{s}$ , compared to a median above  $1\mu\text{s}$  in the case of GJK's best warm-starting strategy. Like the Polyak acceleration, the Nesterov-accelerated GJK algorithm significantly reduces the spread of the distribution of computation times compared to GJK. This is especially visible when using the *OBB WS* strategy together with the Nesterov acceleration. Finally, this benchmark shows that physics simulation strongly benefits from using Nesterov-accelerated GJK warm-started using the *OBB WS* strategy.

## V. CONCLUSION

In this work, we have first established that the well-known GJK algorithm can be understood as a variant of the Frank-Wolfe method, well studied within the convex optimization community, and more precisely, GJK can be identified as a sub-case of fully-corrective Frank-Wolfe. Subsequently, this connection has enabled us to accelerate the GJK algorithm in the sense of Nesterov acceleration by adapting recent contributions on applying Polyak and Nesterov acceleration to the context of Frank-Wolfe. Through extensive benchmarks, we have shown that this acceleration is beneficial for both collision detection and distance computation settings for

scenarios where shapes intersect or are close, accelerating collision detection by up to a factor of two. Interestingly, these two scenarios notably encompass the generic contexts of planning and control as well as physical simulation, which are essential areas of modern robotics. Therefore, although the proposed accelerations correspond to improvements of GJK's execution time on the order of a few microseconds, modern robotics applications may solve millions to billions of collision problems when, for instance, learning a policy with RL [59].

The Polyak and Nesterov accelerations for GJK are already included in the HPP-FCL library [51], notably used by the HPP framework [4] for motion planning, the Pinocchio framework [60] dedicated to simulation and modeling, the Crocodyl [61] and the OSC-2 [62] software dedicated to trajectory optimization, to name a few. In future work, we plan to leverage these accelerated collision detection algorithms in the scope of differentiable collision detection [63], differentiable simulation [64], [65] and constrained optimal control involving contact interactions [61], [66], [67].

Finally, one can expect this work to be largely adopted in the current available GJK implementations, as it only requires minor algorithmic changes. This work should benefit a large audience within robotics (e.g., simulation, planning, control) and beyond by addressing issues shared by other communities, including computer graphics and computational geometry.

#### ACKNOWLEDGMENTS

We warmly thank Francis Bach, Adrien Escande, Joseph Mirabel, and Mehdi Benaïme for fruitful discussions on the various topics covered by this article. We also warmly thank the cohort of developers who contribute to developing open-source, useful, reproducible, and extensible software, which primarily benefits this project and, more widely, the robotics ecosystem.

This work was partly supported by the European Regional Development Fund under the project IMPACT (reg. no. CZ.02.1.01/0.0/0.0/15 003/0000468), by the French government under the management of Agence Nationale de la Recherche as part of the "Investissements d'avenir" program, reference ANR-19-P3IA-0001 (PRAIRIE 3IA Institute), by the AGIMUS project, funded by the European Union under GA no.101070165 - views and opinions expressed are those of the author(s) only and do not necessarily reflect those of the European Union or the European Commission, neither the European Union nor the European Commission can be held responsible for them - and by the Louis Vuitton ENS Chair on Artificial Intelligence.

#### REFERENCES

- [1] E. Coumans and Y. Bai, "Pybullet, a python module for physics simulation for games, robotics and machine learning," 2016.
- [2] Nvidia, "Persistent contact manifold," 2008.
- [3] E. Todorov, T. Erez, and Y. Tassa, "Mujoco: A physics engine for model-based control," in *2012 IEEE/RSJ international conference on intelligent robots and systems*. IEEE, 2012, pp. 5026–5033.
- [4] J. Mirabel, S. Tonneau, P. Fernbach, A.-K. Seppälä, M. Campana, N. Mansard, and F. Lamiraux, "Hpp: A new software for constrained motion planning," in *2016 IEEE/RSJ International Conference on Intelligent Robots and Systems (IROS)*. IEEE, 2016, pp. 383–389.
- [5] M. A. Toussaint, K. R. Allen, K. A. Smith, and J. B. Tenenbaum, "Differentiable physics and stable modes for tool-use and manipulation planning," *Robotics: Science and Systems*, 2018.
- [6] J. Schulman, Y. Duan, J. Ho, A. Lee, I. Awwal, H. Bradlow, J. Pan, S. Patil, K. Goldberg, and P. Abbeel, "Motion planning with sequential convex optimization and convex collision checking," *The International Journal of Robotics Research*, vol. 33, no. 9, pp. 1251–1270, 2014.
- [7] C. Ericson, *Real-time collision detection*. Crc Press, 2004.
- [8] K. Mamou and F. Ghorbel, "A simple and efficient approach for 3d mesh approximate convex decomposition," in *2009 16th IEEE international conference on image processing (ICIP)*. IEEE, 2009, pp. 3501–3504.
- [9] E. Gilbert and D. Johnson, "Distance functions and their application to robot path planning in the presence of obstacles," *IEEE Journal on Robotics and Automation*, vol. 1, no. 1, pp. 21–30, 1985.
- [10] O. Stasse, A. Escande, N. Mansard, S. Miossec, P. Evrard, and A. Kheddar, "Real-time (self)-collision avoidance task on a hrp-2 humanoid robot," in *2008 IEEE international conference on robotics and automation*. IEEE, 2008, pp. 3200–3205.
- [11] M. Frank and P. Wolfe, "An algorithm for quadratic programming," *Naval research logistics quarterly*, vol. 3, no. 1-2, pp. 95–110, 1956.
- [12] E. G. Gilbert, D. W. Johnson, and S. S. Keerthi, "A fast procedure for computing the distance between complex objects in three-dimensional space," *IEEE Journal on Robotics and Automation*, vol. 4, no. 2, pp. 193–203, 1988.
- [13] B. Li, A. Sadeghi, and G. Giannakis, "Heavy ball momentum for conditional gradient," *Advances in Neural Information Processing Systems*, vol. 34, pp. 21 244–21 255, 2021.
- [14] B. Li, M. Coutino, G. B. Giannakis, and G. Leus, "A momentum-guided frank-wolfe algorithm," *IEEE Transactions on Signal Processing*, vol. 69, pp. 3597–3611, 2021.
- [15] D. Fiser, "Github: libccd," <https://github.com/danfis/libccd>, 2010.
- [16] J. Pan, S. Chitta, and D. Manocha, "Github: Fcl – the flexible collision library," 2012.
- [17] E. Coumans, "Github: Bullet physics sdk," <https://github.com/bulletphysics/bullet3>, 2015.
- [18] R. Tedrake and the Drake Development Team, "Drake: Model-based design and verification for robotics," 2019. [Online]. Available: <https://drake.mit.edu>
- [19] R. L. Smith, "Github: The open dynamics engine (ODE)," <https://github.com/thomasmarsh/ODE>, 2001–2007.
- [20] L. Montaut, Q. Lidec, V. Petrík, J. Sivic, and J. Carpentier, "Collision Detection Accelerated: An Optimization Perspective," in *Proceedings of Robotics: Science and Systems*, New York City, NY, USA, June 2022.
- [21] G. v. d. Bergen, "A fast and robust gjk implementation for collision detection of convex objects," *Journal of graphics tools*, vol. 4, no. 2, pp. 7–25, 1999.
- [22] G. Van den Bergen, "Proximity Queries and Penetration Depth Computation on 3D Game Objects," in *Game Developers Conference*, 2001.
- [23] M. C. Lin and J. F. Canny, "A fast algorithm for incremental distance calculation," in *ICRA*, vol. 91, 1991, pp. 9–12.
- [24] B. Mirtich, "V-clip: Fast and robust polyhedral collision detection," *ACM Transactions On Graphics (TOG)*, vol. 17, no. 3, pp. 177–208, 1998.
- [25] S. Cameron, "A comparison of two fast algorithms for computing the distance between convex polyhedra," *IEEE transactions on Robotics and Automation*, vol. 13, no. 6, pp. 915–920, 1997.
- [26] G. Van Den Bergen, *Collision detection in interactive 3D environments*. CRC Press, 2003.
- [27] G. Snethen, "Complex collision made simple," pp. 165–178, 2008.
- [28] J. Pan, S. Chitta, and D. Manocha, "Fcl: A general purpose library for collision and proximity queries," in *2012 IEEE International Conference on Robotics and Automation*. IEEE, 2012, pp. 3859–3866.
- [29] M. Macklin, "Simulation for learning and robotics: Numerical methods for contact, deformation, and identification," Ph.D. dissertation, University of Copenhagen, 2020.
- [30] M. Montanari, N. Petrinic, and E. Barbieri, "Improving the gjk algorithm for faster and more reliable distance queries between convex objects," *ACM Transactions on Graphics (TOG)*, vol. 36, no. 3, pp. 1–17, 2017.
- [31] J. Canny, "Collision detection for moving polyhedra," *IEEE Transactions on Pattern Analysis and Machine Intelligence*, no. 2, pp. 200–209, 1986.
- [32] X. Qin and N. T. An, "Smoothing algorithms for computing the projection onto a minkowski sum of convex sets," *Computational Optimization and Applications*, vol. 74, no. 3, pp. 821–850, 2019.
- [33] E. G. Gilbert, "An iterative procedure for computing the minimum of a quadratic form on a convex set," *SIAM Journal on Control*, vol. 4, no. 1, pp. 61–80, 1966.
- [34] P. Wolfe, "Finding the nearest point in a polytope," *Mathematical Programming*, vol. 11, pp. 128–149, 1976.



- [35] A. d'Aspremont, D. Scieur, A. Taylor *et al.*, "Acceleration methods," *Foundations and Trends® in Optimization*, vol. 5, no. 1-2, pp. 1–245, 2021.
- [36] D. Garber and E. Hazan, "Playing non-linear games with linear oracles," in *2013 IEEE 54th annual symposium on foundations of computer science*. IEEE, 2013, pp. 420–428.
- [37] J. Guélat and P. Marcotte, "Some comments on wolfe's 'away step,'" *Mathematical Programming*, vol. 35, no. 1, pp. 110–119, 1986.
- [38] M. Jaggi, "Revisiting frank-wolfe: Projection-free sparse convex optimization," in *International conference on machine learning*. PMLR, 2013, pp. 427–435.
- [39] T. Kerdreux, A. d'Aspremont, and S. Pokutta, "Projection-free optimization on uniformly convex sets," in *International Conference on Artificial Intelligence and Statistics*. PMLR, 2021, pp. 19–27.
- [40] S. Lacoste-Julien and M. Jaggi, "On the global linear convergence of frank-wolfe optimization variants," *Advances in neural information processing systems*, vol. 28, 2015.
- [41] Y. E. Nesterov, "A method of solving a convex programming problem with convergence rate  $\mathcal{O}(k^{-2})$ ," in *Doklady Akademii Nauk*, vol. 269, no. 3. Russian Academy of Sciences, 1983, pp. 543–547.
- [42] J. Nocedal and S. J. Wright, *Numerical optimization*. Springer, 1999.
- [43] F. Bach *et al.*, "Learning with submodular functions: A convex optimization perspective," *Foundations and Trends® in Machine Learning*, vol. 6, no. 2-3, pp. 145–373, 2013.
- [44] S. Boyd and L. Vandenberghe, *Convex Optimization*. Cambridge University Press, 2004.
- [45] C. A. Holloway, "An extension of the frank and wolfe method of feasible directions," *Mathematical Programming*, vol. 6, pp. 14–27, 1974.
- [46] T. Kerdreux, A. d'Aspremont, and S. Pokutta, "Restarting frank-wolfe," in *The 22nd international conference on artificial intelligence and statistics*. PMLR, 2019, pp. 1275–1283.
- [47] G. Dantzig, *Linear programming and extensions*. Princeton university press, 2016.
- [48] C. Carathéodory, "Über den variabilitätsbereich der koeffizienten von potenzreihen, die gegebene werte nicht annehmen," *Mathematische Annalen*, vol. 64, no. 1, pp. 95–115, 1907.
- [49] B. T. Polyak, "Some methods of speeding up the convergence of iteration methods," *Ussr computational mathematics and mathematical physics*, vol. 4, no. 5, pp. 1–17, 1964.
- [50] A. Bambade, S. El-Kazdadi, A. Taylor, and J. Carpentier, "Prox-qp: Yet another quadratic programming solver for robotics and beyond," in *RSS 2022-Robotics: Science and Systems*, 2022.
- [51] J. Pan, S. Chitta, D. Manocha, F. Lamiroux, J. Mirabel, J. Carpentier *et al.*, "Hpp-fcl: an extension of the flexible collision library," <https://github.com/humanoid-path-planner/hpp-fcl>, 2015–2022.
- [52] B. Calli, A. Singh, A. Walsman, S. Srinivasa, P. Abbeel, and A. M. Dollar, "The ycb object and model set: Towards common benchmarks for manipulation research," in *2015 international conference on advanced robotics (ICAR)*. IEEE, 2015, pp. 510–517.
- [53] B. Stellato, G. Banjac, P. Goulart, A. Bemporad, and S. Boyd, "Osqp: An operator splitting solver for quadratic programs," *Mathematical Programming Computation*, vol. 12, no. 4, pp. 637–672, 2020.
- [54] D. Goldfarb and A. Idnani, "A numerically stable dual method for solving strictly convex quadratic programs," *Mathematical programming*, vol. 27, no. 1, pp. 1–33, 1983.
- [55] A. Wächter and L. T. Biegler, "On the implementation of an interior-point filter line-search algorithm for large-scale nonlinear programming," *Mathematical programming*, vol. 106, pp. 25–57, 2006.
- [56] K. Tracy, T. A. Howell, and Z. Manchester, "Differentiable collision detection for a set of convex primitives," 2022.
- [57] B. Brogliato, A. Ten Dam, L. Paoli, F. Génot, and M. Abadie, "Numerical simulation of finite dimensional multibody nonsmooth mechanical systems," *Appl. Mech. Rev.*, vol. 55, no. 2, pp. 107–150, 2002.
- [58] Q. L. Lidec, W. Jallet, L. Montaut, I. Laptev, C. Schmid, and J. Carpentier, "Contact models in robotics: a comparative analysis."
- [59] I. Akkaya, M. Andrychowicz, M. Chociej, M. Litwin, B. McGrew, A. Petron, A. Paino, M. Plappert, G. Powell, R. Ribas *et al.*, "Solving rubik's cube with a robot hand," *arXiv preprint arXiv:1910.07113*, 2019.
- [60] J. Carpentier, G. Saurel, G. Buondonno, J. Mirabel, F. Lamiroux, O. Stasse, and N. Mansard, "The pinocchio c++ library: A fast and flexible implementation of rigid body dynamics algorithms and their analytical derivatives," in *2019 IEEE/SICE International Symposium on System Integration (SII)*. IEEE, 2019, pp. 614–619.
- [61] C. Mastalli, R. Budhiraja, W. Merkt, G. Saurel, B. Hammoud, M. Naveau, J. Carpentier, L. Righetti, S. Vijayakumar, and N. Mansard, "Crocodyl: An efficient and versatile framework for multi-contact optimal control," in *2020 IEEE International Conference on Robotics and Automation (ICRA)*. IEEE, 2020, pp. 2536–2542.
- [62] F. Farshidian *et al.*, "Optimal control for switched systems," <https://github.com/leggedrobotics/ocs2>, 2018.
- [63] L. Montaut, Q. L. Lidec, A. Bambade, V. Petrik, J. Sivic, and J. Carpentier, "Differentiable collision detection: a randomized smoothing approach," in *2023 IEEE International Conference on Robotics and Automation (ICRA)*, 2022.
- [64] K. Werling, D. Omens, J. Lee, I. Exarchos, and C. K. Liu, "Fast and feature-complete differentiable physics engine for articulated rigid bodies with contact constraints," in *Robotics: Science and Systems*, 2021.
- [65] Q. Le Lidec, I. Laptev, C. Schmid, and J. Carpentier, "Differentiable rendering with perturbed optimizers," *Advances in Neural Information Processing Systems*, vol. 34, pp. 20 398–20 409, 2021.
- [66] R. Budhiraja, J. Carpentier, C. Mastalli, and N. Mansard, "Differential dynamic programming for multi-phase rigid contact dynamics," in *2018 IEEE-RAS 18th International Conference on Humanoid Robots (Humanoids)*. IEEE, 2018, pp. 1–9.
- [67] W. Jallet, A. Bambade, N. Mansard, and J. Carpentier, "Constrained differential dynamic programming: A primal-dual augmented lagrangian approach," in *2022 IEEE/RSJ International Conference on Intelligent Robots and Systems (IROS)*. IEEE, 2022, pp. 13 371–13 378.